

POLITECNICO DI TORINO

Collegio di Ingegneria Meccanica, Aerospaziale, dell'Autoveicolo e della
Produzione

**Corso di Laurea Magistrale
in Ingegneria Meccanica**

Tesi di Laurea Magistrale

Exhaust gas study of diesel engines by CFD 3D analysis to evaluate the correct NOx sensor reading



Relatore

prof. Daniela Misul

Candidato

Salvatore Contrafatto

Luglio 2019

INDEX

| | |
|--|-----------|
| SOMMARIO | 5 |
| ABSTRACT | 7 |
| INTRODUCTION | 9 |
| 1. COMPUTATIONAL FLUID DYNAMICS (CFD) | 11 |
| 1.1. STEP 1 | 11 |
| 1.2. STEP 2 | 12 |
| 1.3. STEP 3 | 12 |
| 1.4. STEP 4 | 12 |
| 2. THE BASIC EQUATIONS OF FLUID DYNAMICS | 15 |
| 2.1. THE MASS CONSERVATION EQUATION | 16 |
| 2.2. THE MOMENTUM CONSERVATION LAW OR EQUATION OF MOTION | 16 |
| 2.3. THE ENERGY CONSERVATION EQUATION | 17 |
| 2.4. PASSIVE SCALARS | 19 |
| 2.5. POROUS MEDIA | 19 |
| 3. THE DYNAMICAL LEVEL OF APPROXIMATION | 21 |
| 3.1. DIRECT NUMERICAL SIMULATION (DNS) | 21 |
| 3.2. LARGE EDDY SIMULATION (LES) | 22 |
| 3.3. REYNOLDS AVERAGED NAVIER-STOKES EQUATIONS (RANS) | 22 |
| 4. BASIC DISCRETIZATION TECHNIQUES | 23 |
| 4.1. FINITE DIFFERENCE METHOD (FDM) | 23 |
| 4.2. FINITE VOLUME METHOD (FVM) | 26 |
| 4.3. MESH GENERATION | 28 |
| 5. TURBULENCE MODELS | 31 |
| 5.1. THE K-EPSILON MODEL | 32 |
| 5.2. THE K- Ω MODEL | 33 |
| 6. LAGRANGIAN MULTIPHASE FLOW | 37 |
| 6.1. THE DRAG FORCE | 38 |
| 6.2. PRESSURE GRADIENT FORCE | 38 |
| 6.3. PARTICLE POSITION AND VELOCITY | 38 |
| 6.4. TURBULENT DISPERSION | 38 |
| 6.5. PARTICLE MASS BALANCE | 39 |
| 6.6. DROPLET EVAPORATION | 39 |
| 6.7. TWO-WAY COUPLING WITH THE CONTINUOUS PHASE | 39 |
| 6.8. PARTICLE INJECTION | 39 |
| 6.9. PARTICLE SIZE DISTRIBUTION | 40 |
| 6.10. TAB BREAKUP | 40 |
| 6.11. WALL IMPINGEMENT | 40 |
| 6.12. BAI-GOSMAN WALL IMPINGEMENT | 40 |
| 6.12.1. PARCEL | 42 |
| 7. AFTER TREATMENT SYSTEMS | 45 |
| 7.1. SELECTIVE CATALYTIC REDUCTION (SCR) | 45 |
| 8. PASSIVE SCALAR TRACER METHOD | 49 |
| 9. PASSIVE SCALAR TRACER METHOD – FIRST APPLICATION | 57 |
| 9.1. BASELINE CONFIGURATION | 58 |
| 9.2. CONE CONFIGURATION | 61 |
| 9.3. BAFFLE CONFIGURATION | 64 |
| 9.4. GENERAL CONCLUSIONS | 66 |

| | |
|--|-----------|
| 10. PASSIVE SCALAR TRACER METHOD - SECOND APPLICATION | 69 |
| 10.1. K-E MODEL ANALYSIS | 70 |
| 10.2. K - Ω MODEL ANALYSIS | 72 |
| 11. NH3 INJECTION SIMULATION | 75 |
| 11.1. STEADY STATE INJECTION | 75 |
| 11.2. UNSTEADY STATE INJECTION | 77 |
| 12. NOX DISTRIBUTION AT SCR OUTLET - MIXING | 79 |
| CONCLUSION | 83 |
| BIBLIOGRAPHY: | 84 |

Sommario

In questo trattato di tesi magistrale, è stato studiato il problema della lettura del sensore NOx posto a valle dei sistemi di post trattamento (ATS) dei motori diesel. Lo studio è stato effettuato tramite l'uso della fluidodinamica computazionale (CFD), simulando il flusso di gas esausti all'interno di questi sistemi. Il software utilizzato è il software commerciale STAR CCM+. Lo scopo è quello di trovare una metodologia che fornisca, in maniera più o meno accurata, un indicatore di rischio del posizionamento del sensore NOx. Questo rischio si basa sostanzialmente sulla capacità più o meno buona del flusso di miscelarsi una volta uscito dal riduttore catalitico selettivo (SCR), e dalla distribuzione degli NOx nella sezione di quest'ultimo. Si è cercato di simulare il comportamento derivante da questi due fattori.

Le analisi CFD sono state svolte su più di una geometria. Il metodo degli scalari passivi o dei traccianti (passive scalars method or tracers method) è stato utilizzato per valutare il corretto miscelamento del fluido. Una iniezione semplificata invece ha permesso di ricavare una "reale" distribuzione di NH₃ all'ingresso dell'SCR. Da questa successivamente è stata imposta una distribuzione di NOx all'uscita dell'SCR e il suo mescolamento nuovamente analizzato.

Il metodo si può ritenere affidabile se rispetta i target imposti, quindi il sensore NOx non sarà affetto da lettura se posizionato in zone dove il mescolamento è abbastanza elevato.

Abstract

In this master thesis treatise, the problem of reading the NO_x sensor downstream of the after-treatment systems (ATS) of diesel engines was studied. The study was carried out using computational fluid dynamics (CFD), simulating the flow of exhaust gases within these systems. The software used is the commercial software STAR CCM+. The aim is to find a methodology that provides, in a more or less accurate way, a risk indicator of the positioning of the NO_x sensor. This risk is essentially based on the more or less good capacity of the flow to mix once it is released from the selective catalytic reducer (SCR), and from the distribution of NO_x in the latter section. It tried to simulate the behaviour deriving from these two factors.

The CFD analysis were performed on more than one geometry. The method of passive scalars or tracers (passive scalars method or tracers method) was used to evaluate the correct mixing of the fluid. A simplified injection, on the other hand, made it possible to derive a "real" distribution of NH₃ at the entrance of the SCR. From this it was subsequently imposed a NO_x distribution at the SCR outlet and its mixing again analysed.

The method can be considered reliable if it respects the imposed targets, therefore the NO_x sensor will not be affected by reading if positioned in areas where the mixing is quite high.

Introduction

Air pollution has become an important problem with the pass of the years, and the greatest automotive producers are constantly challenged by the pressing emission law, which, almost every year, reduce the target of emissions to reach. Small modifications, or simply push to the limit the after treatment system, could generate many problems, which before are not manifested. For Diesel engine, the main problem after PM, is the NO_x emission. The tendency is to reduce almost to zero the NO_x and in order to do so, some technologies was developed during time. One of them is the “Selective Catalyst Reduction” (SCR), in which, through the injection of urea, occurs a NO_x reduction .To reach the limit of NO_x emission, must be injected the right quantity of urea. The system is controlled by a NO_x sensor located at SCR outlet pipe. It is quite obvious that the functioning of the system depends on a correct reading made by the sensor, and different analysis must be done to place correctly the sensor.

Studying the gas flow is not simple, as thermo-fluid dynamics analysis of the components must be done, and a lot of differential equations involving fluid flow are computed by means computational fluid dynamics (CFD) software. One of these is STAR CCM+, used for the simulation done for this work.

The purpose of the work was to find a CFD methodology to understand why some NO_x sensor are affected by errors during test bench, a methodology that can provide a percentage of the risk of sensor placement. The factors that influence the NO_x sensor reading are mainly two:

- How strong/weak is the mixing before reaching the sensor location;
- How good/bad is the NO_x distribution at SCR outlet section.

These two factors will be analysed, and different models will be created to simulate the impact that they have on sensor reading. The first factor will be analysed using a tracer method, which essentially involves the use of passive scalars inside the fluid flow which simulate the NO_x distribution and their mixing. A sensitivity analysis will be done for the number of passive scalars to use and the shape of the passive scalar input. Different geometry and configuration will be use for this analysis. A particular coefficient that provides the grade of mixing was defined and used as discriminant value with other coefficients like uniformity index.

The second factor, instead will be evaluated with a simulation of the urea injection inside the after treatment system. No chemistry and no fluid film will be consider, but a simple injection was imposed, with the purpose to acquire a hypothetical NO_x distribution for the necessary analysis. Particular attention need to do here because the NO_x distribution strongly depends on NH₃ distribution at SCR inlet, and the input parameters, different models used, particular boundary conditions influence the distribution.

The distribution thus obtained was set up as unique NO_x tracer species from SCR outlet section of another application. The final aim of CFD analysis is to build a reliable model that could confirm the results of test bench.

1. Computational Fluid Dynamics (CFD)

Computational fluid dynamics or CFD is the analysis of systems involving fluid flow, heat transfer and associated phenomena such as chemical reactions by means of computer-based simulation. This technique is very powerful for industrial and non-industrial application areas such as:

- Aerodynamics of vehicles
- Hydrodynamics of ships
- Flows inside rotating passage, diffusers etc.
- Chemical process engineering

The developments of CFD began with the advent of digital computer, becoming a vital component in the design of industrial products and process (for example, the methods have been applied to the design of internal combustion engines, combustion chambers of gas turbine and furnaces). The ultimate aim of improvements of CFD fields is to provide a capability comparable with other CAE (computer-aided engineering) tools like stress analysis code.

Investment on this field are comparable with the cost of a high-quality experimental facility, but there are several advantages of CFD over experiment-based approaches to fluid systems design:

- Substantial reduction of lead times and costs of new designs
- Ability to study systems where controlled experiments are difficult or impossible to perform
- Ability to study systems under hazardous conditions at and beyond their normal performance limits
- Practically unlimited level of detail of results

The variable cost of an experiment, in terms of facility hire and/or person-hour costs, is proportional to the number of data points and the number of configurations tested. In contrast, CFD codes can produce extremely large volumes of results at virtually no added expense, and it is very cheap to perform parametric studies, for instance to optimize equipment performance.

It is possible to itemize the main components of a CFD system and define some steps to follow. These steps are:

- Step 1: It selects the mathematical model, defining the level of approximation to reality that will be simulated.
- Step 2: It covers the discretization phase, which has two main components, the space discretization, defined by the grid generation and the equation discretization, defined by the numerical scheme.
- Step 3: Analyse the numerical scheme and establish its stability and accuracy.
- Step 4: The solution of the numerical scheme has to be obtained by selecting the most appropriate time integration methods.
- Step 5: Graphic post-processing of the numerical data to understand and interpret the physical properties of the obtained simulation results.

Look these steps more in detail.

1.1. Step 1

The Navier-Stokes equations are known since 19th century, but they form a system of nonlinear partial differential equations and they are extremely complicated. The major

consequences of this nonlinearity are shock waves, unsteadiness of flows, possible multiple solution etc.

The essential fact to remember at this stage is that within the world of continua, as currently applied to describe the macroscopic behaviour of fluids, there is always an unavoidable level of empiricism in the models. It is therefore important take notice already that any modelling assumption will be associated with generally undefined level of error when compared to the real world.

Need to keep in mind that a good understanding of the physical properties and limitation is important and the discrepancy between CFD predictions and experiments is because theoretical models assumptions might not be adequate to describe the real physics.

1.2. Step 2

Since the computer recognize only numbers, the geometrical and mathematical model must be translated into numbers. This process is called “discretization”. The first action is to discretize the space; the real space continuity of the fluid domain must be replaced with isolated points in space. This set of points is called “grid” or “mesh”. This process of grid generation is very complex and can be very delicate and time consuming.

Grid generation is a major step in setting up a CFD simulation and its accuracy can be extremely dependent on the grid properties and quality. The whole objective of the simulation is for the computer to provide the numerical values of all relevant flow variables at the positions of the mesh points. Without a grid, there is no possibility to start a CFD simulation.

Once a grid is available, it is possible to initiate the discretization of the mathematical models equations. As the mesh point values are the sole quantities available to the computer, all mathematical operators, such as partial derivatives of the various quantities, will have to be transformed, by the discretization process, into arithmetic operations on the mesh point values.

1.3. Step 3

After discretization, a set of algebraic relations between neighbouring mesh point values is obtained, this relation is called “numerical scheme”.

This scheme must satisfy a certain number of rules and conditions to establish a certain level of accuracy. However, any discretization will generate errors, consequence of the replacement of the continuum model by its discretization.

1.4. Step 4

The solution algorithms depend on the type of problem we are simulating (i.e. time-dependent or steady flows). For time-dependent numerical formulations, a particular attention has to be given to the time integration as not all the time integration schemes are acceptable.

At the end of the discretization process, all numerical schemes finally result in an algebraic system of equations, with as many equations as unknowns.

Obtained the numerical solution it have to manipulate this values through powerful visualization systems such as Cartesian plot for the distribution of a selected quantity in function of a coordinate direction, colour plots of a given quantity in the flow field, streamlines, local values, various animation.

2. The basic Equations of Fluid Dynamics

In nature is possible to see many different types of flow in many different situations, with phenomena like turbulence, which is the main cause of instability of a flow. To write an equation that describes these flows can be very complex. The CFD applications can also lead to a new approach of looking at the laws of fluid mechanics. The mathematical forms how they can be written are various, but it is important to take a close look at a specific form of these laws, through the concept of *conservation laws*.

Given a generic quantity U , the conservation law of this quantity can state as follow:

The variation of the total amount of a quantity U inside a given domain is equal to the balance between the amount of that quantity entering and leaving the considered domain, plus the contributions from eventual sources generating that quantity.

The laws describing the fluid dynamics are totally defined by the conservation of the following three quantities:

1. Mass;
2. Momentum;
3. Energy.

This represents in total five equations, as the momentum, defined as the product of density and velocity, is a vector with three components in space. It is essential to keep in mind that other quantities like temperature, pressure, entropy, do NOT satisfy the conservation law. This does not mean that it is impossible to write an equation for this quantity, it just means that the aforementioned equation will not be in the form of a conservation law.

Before to proceed with the equations of these quantities, it is good to know that there are two mathematical forms to write the conservation law:

- One is called integral form and is the most general expression of a conservation law:
 - It is valid for any fixed surface and volume;
 - In absence of source, the internal variation depends only on the flux contributions through the surface S and not on the flux values inside the volume.
 - The fluxes may be discontinuous because they do not appear under derivative or gradient (case of shock waves)
- The other is called differential form of the conservative law, and can be found applying the Gauss' theorem to the surface integral term of the fluxes and the surface of the sources, assuming that these fluxes and surface sources are continuous:
 - The fluxes appear exclusively under gradient operator (only space derivative term).
 - This indicates the way to recognize a conservative law in differential form. If the space derivative terms can be grouped as a divergence operator, the equation is in conservative form. If not the equation is in 'non-conservative', or 'quasi-linear' form.
 - More restrictive than integral form, because the fluxes need to be differentiable

In the following paragraphs are described the basic equations that rule the fluid dynamics. Together, mass, momentum and energy equation, applied to a viscous fluid, are known as the Navier-Stokes equations.

2.1. The Mass Conservation Equation

The equation of mass conservation, also called the *continuity equation*, is a general statement of kinematic nature. It expresses the empirical fact that in a fluid system, mass cannot disappear from the system, nor be created. No diffusive flux exists for the mass transport, which means that mass can only be transported through convection. The integral form can be write as follow:

$$\frac{\partial}{\partial t} \int_{\Omega} \rho d\Omega + \oint_S \rho \vec{v} \cdot d\vec{S} = 0 \quad (2.1)$$

Moreover, in differential form following:

$$\frac{\partial \rho}{\partial t} + \vec{\nabla} \cdot (\rho \vec{v}) = 0 \quad (2.2)$$

It is possible to introduce the material or total derivative by working out the divergence operator, leading to:

$$\frac{d\rho}{dt} + \rho \vec{\nabla} \cdot \vec{v} = 0 \quad (2.3)$$

Where the material or total derivative is:

$$\frac{d}{dt} \triangleq \frac{\partial}{\partial t} + \vec{v} \cdot \vec{\nabla} \quad (2.4)$$

While the integral is in a conservative form or in a divergence form, developing the divergence gives an equation that is in a quasi-linear or non-conservative form. The discretization of a quasi-linear form as equation (continuity with material derivative) will lead the numerical scheme to not keep the total mass constant.

The material derivative plays an important role in fluid mechanics; it is interesting to catch the physical significance. Looking from a fixed point at a body in motion it is possible to notice the change after a short time step, describing by $\frac{d}{dt}$. If it follows the body in its movement, there is an additional variation due to motion of the fluid. The total variation can be obtained by adding this contribution to the local one $\frac{d}{dt}$. This sum is called the material or total derivative defined by the equation (material derivative)

For an incompressible fluid, the density is constant and the continuity equation reduces to the divergence free condition for the velocity

$$\vec{\nabla} \cdot \vec{v} = 0 \quad (2.5)$$

2.2. The momentum conservation law or equation of motion

Momentum is a vector quantity defined as the product of mass and velocity, which becomes, when expressed per unit of volume, the product of density and velocity. In order to determine all the terms of the conservation equations, it is necessary to define the sources influencing the variation of momentum, which are the forces acting on the system. These ones consist in the external forces and internal forces defined per unit mass. All these forces, added at variation of momentum and its convection, constitute the motion equation.

The equation of motion is state as follow:

$$\frac{\partial}{\partial t} \int_{\Omega} \rho \vec{v} d\Omega + \oint_S \rho \vec{v} (\vec{v} \cdot d\vec{S}) = \int_{\Omega} \rho \vec{f}_e d\Omega + \oint_S \underline{\underline{\sigma}} \cdot d\vec{S} \quad (2.6)$$

Where the first term on the left hand side is the variation of the momentum, and the second term is the convection of the momentum. The first term on the right hand side are the external forces. These forces can be gravity, electromechanical forces etc. The last term represent the

internal forces of the fluid, it is the internal stress tensor, composed by the pressure and the viscous shear stress:

$$\underline{\underline{\sigma}} = -p\underline{\underline{I}} + \underline{\underline{\tau}} \quad (2.7)$$

$\underline{\underline{I}}$ is the unit tensor, p is the isotropic pressure and $\underline{\underline{\tau}}$ the viscous shear stress equal to:

$$\tau_{ij} = \mu \left[\left(\frac{\partial v_j}{\partial x_i} + \frac{\partial v_i}{\partial x_j} \right) - \frac{2}{3} (\nabla \cdot \mathbf{v}) \delta_{ij} \right] \quad (2.8)$$

Where μ is the dynamic viscosity. This relation is valid for Newtonian fluid.

It is important to remember that the viscous shear stresses represent the internal friction force of fluid layers against each other.

Working up on divergence of the integral form it is possible to write the differential form as follow:

$$\frac{\partial \rho \vec{v}}{\partial t} + \nabla \cdot (\rho \vec{v} \otimes \vec{v} + p\underline{\underline{I}} - \underline{\underline{\tau}}) = \rho \vec{f}_e \quad (2.9)$$

In addition, introducing the total derivative:

$$\rho \frac{d\vec{v}}{dt} \equiv \rho \frac{\partial \vec{v}}{\partial t} + \rho (\vec{v} \cdot \nabla) \vec{v} = -\nabla p + \nabla \cdot \underline{\underline{\tau}} + \rho \vec{f}_e \quad (2.10)$$

The convective term in either the form in the second term of the last two equation is nonlinear even for incompressible flows. This is important because this term is in particular the cause of the appearance of turbulence.

2.3. The energy conservation equation

In a system, the energy content is measured by its internal energy per unit mass e . This internal energy is a state variable and depends only on the final and initial states. The conserved *total energy* is defined as the sum of its internal energy and its kinetic energy per unit mass $\frac{v^2}{2}$. The total energy E per unit mass is defined as follow:

$$E = e + \frac{\vec{v}^2}{2} \quad (2.11)$$

The first law of thermodynamic states that the sources for the variation of the total energy are the work of the forces acting on the system plus the heat transmitted to the system. As it was done for the other two equation, the sum of all contribution (convective, diffusive flux) becomes the integral form of the energy conservation equation, with the difference here that the forces acting on volume and on surface are sources of heat:

$$\frac{\partial}{\partial t} \int_{\Omega} \rho E d\Omega + \oint_S \rho E \vec{v} \cdot d\vec{S} = \oint_S k \vec{\nabla} T \cdot d\vec{S} + \int_{\Omega} (\rho \vec{f}_e \cdot \vec{v} + q_H) d\Omega + \oint_S (\underline{\underline{\sigma}} \cdot \vec{v}) \cdot d\vec{S} \quad (2.12)$$

After transformation to volume integrals, the differential form of the conservation equation for energy becomes

$$\frac{\partial \rho E}{\partial t} + \vec{\nabla} \cdot (\rho E \vec{v}) = \vec{\nabla} \cdot (k \vec{\nabla} T) + \vec{\nabla} \cdot (\underline{\underline{\sigma}} \cdot \vec{v}) + W_f + q_H \quad (2.13)$$

W_f is the work of the external volume forces

$$W_f = \rho \vec{f}_e \cdot \vec{v} \quad (2.14)$$

The term with the gradient of temperature is better known as the *Fourier's law* of heat conduction:

$$\vec{q} = -k\vec{\nabla}T \quad (2.15)$$

Where \vec{q} is the flux of heat in $\frac{W}{m^2}$, k is the thermal conductivity coefficient $k = \rho \cdot c_p \kappa$ (where κ is the thermal diffusivity coefficient) $\kappa = \mu \cdot \frac{c_p}{Pr}$, with Pr is the Prandtl number $Pr = \frac{\nu}{\kappa} = \mu \cdot \frac{c_p}{k}$. Introducing the enthalpy of the fluid $h = \left(e + \frac{p}{\rho}\right)$, leads to the following alternative expression in differential form:

$$\frac{\partial \rho E}{\partial t} + \vec{\nabla} \cdot \left(\rho \vec{v} H - k \vec{\nabla} T - \underline{\underline{\tau}} \cdot \vec{v} \right) = W_f + q_H \quad (2.16)$$

Where the stagnation, or total, enthalpy H is introduced

$$H = e + \frac{p}{\rho} + \frac{\vec{v}^2}{2} = h + \frac{\vec{v}^2}{2} = E + \frac{p}{\rho} \quad (2.17)$$

It is possible to obtain an equation for the variation of the internal energy e , introducing the viscous dissipation rate ε_V :

$$\varepsilon_V = \left(\underline{\underline{\tau}} \cdot \vec{\nabla} \right) \cdot \vec{v} = \frac{1}{2\mu} \left(\underline{\underline{\tau}} \otimes \underline{\underline{\tau}}^T \right) = \tau_{ij} \frac{\partial v_i}{\partial x_j} \quad (2.18)$$

This leads to

$$\frac{\partial \rho e}{\partial t} + \vec{\nabla} \cdot (\rho \vec{v} h) = (\vec{v} \cdot \vec{\nabla}) p + \vec{\nabla} \cdot (k \vec{\nabla} T) + \varepsilon_V + q_H \quad (2.19)$$

Observe that the term W_f representing the work of the external force and does not contribute to the internal energy balance. Indeed, this equation is not in conservation form, since the pressure term is not under the form of a divergence. The introduction of the continuity equation leads to:

$$\rho \frac{de}{dt} = -p(\vec{v} \cdot \vec{\nabla}) + \vec{\nabla} \cdot (k \vec{\nabla} T) + \varepsilon_V + q_H \quad (2.20)$$

The first term is the reversible work of the pressure forces (and vanishes in an incompressible flow), while the other terms are being considered as heat additions, with the dissipation term ε_V acting as an irreversible heat source. This appears clearly by introducing the entropy per unit mass of the fluid, through the thermodynamic relation

$$T ds = de + p d \left(\frac{1}{\rho} \right) = dh - \frac{dp}{\rho} \quad (2.21)$$

The separation between reversible and irreversible heat additions is defined by

$$T ds = dq + dq' \quad (2.22)$$

Where dq is a reversible heat transfer to the fluid, while dq' is an irreversible heat addition. From the second principle of thermodynamics, dq' is always non-negative and hence in an adiabatic flow ($dq = 0$), with irreversible transformations, the entropy will always increase. Introducing the thermodynamic equation in the alternative form of internal energy, it obtains:

$$\rho T \frac{ds}{dt} = \varepsilon_V + \vec{\nabla} \cdot (k \vec{\nabla} T) + q_H \quad (2.23)$$

Where the last two terms can be considered as reversible heat additions by conduction and by other sources. Therefore, in an adiabatic flow, $q_H = 0$, without heat conduction ($k = 0$) the non-negative dissipation term ε_V behaves as a non-reversible heat sources. This is the entropy equation of the flow. Although this equation plays an important role, it is not independent from the energy equation. Only one of these has to be added to the conservation laws for mass and momentum. In addition, the entropy is not a conserved quantity in the sense of the previously derived conservation equations.

2.4. Passive Scalars

Passive scalars are user-defined variables of arbitrary value, assigned to fluid phases or individual particles. They are passive because they do not affect the physical properties of the simulation. An intuitive way to think of passive scalars is as tracer dye in a fluid, but with numerical values instead of colours, and with no appreciable mass or volume. It is possible to use more than a passive scalar in a simulation, for examples where this capability can be useful:

- Choosing the best position for a sensor while designing a part with multiple inlet pipes and an exhaust pipe. The passive scalars can be used to check the scalar values at discrete points in the computational domain. Then it can be determined which of the scalars send the strongest signal to the sensor.
- Analysing the mixing of two fluid streams that have the same properties. The fluid is represented as single-phase, but can use multiple passive scalars to examine the effect of mixing.
- Tracing how smoke or any other vapour would convect and diffuse in a room or any fluid domain. More specifically, it can be modelled the dissolution of a gas in a liquid.

The transport equation for the passive scalar component ϕ_j is:

$$\frac{\partial}{\partial t} \int_{\Omega} \rho \phi_i d\Omega + \oint_S \rho \phi_i (\vec{v} \cdot d\vec{S}) = \int_{\Omega} S_{o\phi_i} d\Omega + \oint_S \vec{j}_i \cdot d\vec{S} \quad (2.25)$$

Where i is the component index, \vec{j}_i is the diffusion flux, $S_{o\phi_i}$ is a source term for passive scalar component i , ϕ_i is assumed to be positive-definite.

The diffusion flux is defined:

$$\vec{j}_i = \left(\frac{\mu}{\sigma} + \frac{\mu_t}{\sigma_t} \right) \vec{\nabla} \phi_i \quad (2.26)$$

Where μ is the viscosity, μ_t is the turbulent viscosity, σ is molecular Schmidt number-a material property, σ_t is the turbulent Schmidt number.

2.5. Porous media

Porous media are continua that contain both fluid and fine-scale solid structures, for example: radiators, filters, honeycomb structures, or fibrous materials. The solid geometrical structures are too fine to be individually meshed and fully resolved by a computational grid. The effects of the porous medium on the flow can be written using the Darcy's law for diffusion, correlating the pressure loss on porous region and the flow that through the porous medium:

$$\vec{F}_Q = -\frac{k}{\mu} \vec{\nabla} p \quad (2.27)$$

If the Reynold number is higher than about 1 to 10, the inertial can also become significant. So an inertial term called as Forchheimer term, is added at the Darcy's law, and the pressure loss per length unit can be write:

$$\frac{\partial p}{\partial x} = -\frac{\mu}{k} \vec{F}_Q - \frac{\rho}{k_1} \vec{F}_Q^2 \quad (2.28)$$

This equation is called the Darcy-Forchheimer law. Work on this equation it can be write the Darcy-Forchheimer law like this:

$$\Delta p = -\rho(P_i |v| + P_v)v \quad (2.29)$$

Where P_i is the porous inertial resistance and the P_v is the porous viscous resistance. With this model, it is possible to avoid simulating the porous media and taking in account its effects on the flow that through the porous region.

3. The dynamical level of approximation

Discussed the basic equations of fluid dynamics that all together are known as the system of Navier-Stokes equations, it is important now to reduce the complexity of this system, based on physical considerations, connected to the dynamical properties of fluid flows.

The complexity levels of these equations are many:

- The NSF are a system of five equations time-dependent partial differential *fully coupled*, this happens through the velocity or density fields, possibly the thermal field when thermal effects are significant.
- Each equation is *nonlinear*. This is not a just a mathematical observation, but it has major consequences on the whole of fluid mechanics:
 - Dominant nonlinearity is provided by the convection term, responsible for the appearance of turbulence, which is a spontaneous instability of the flow, whereby all quantities take up a statistical (chaotic) behaviour.
 - For compressible flow, the nonlinearity leads to the existence of shock waves on supersonic flow. The physical quantity are subjected to discontinuous jump and these are indeed exact solutions of the nonlinear inviscid Euler equations.
 - Flow thermal nonlinearities appear such as Bénard cells in shallow heated fluid layers, representative of complex thermal convection phenomena.
 - Flows with free surfaces provides nonlinearity (breaking of waves). Also in two phase flows the nonlinearities of thermodynamic origin lead to phase changes (evaporation, condensation).
 - Non-unique solutions can be found from nonlinearities.

For these and many other complexities, the CFD presents different approximation levels based on accuracy of the solution desired and the capacity of the computing power available. They are the Direct Numerical Simulation (DNS), Large Eddy Simulation (LES) and Reynolds Averaged Navier-Stokes (RANS).

Before to describe these approximations, it is important to specify that in a CFD application, it should evaluate and define the time and length scales at which it wants to model the flow system, in the same way the experimentalists choose their instrumentation in function of the level of details they require.

3.1. Direct Numerical Simulation (DNS)

Turbulence is a fundamental property of fluid mechanics. Any flow system will remain laminar up to a certain critical value of the Reynolds number. Above this value, all flows become turbulent, characterized by the appearance of statistical fluctuations of the variables around mean values.

The DNS has as objective to simulate on computer the whole range of turbulent statistical fluctuations at all relevant physical scales. The size of the smallest turbulent eddies is inversely proportional to $Re^{\frac{3}{4}}$, if it wishes a resolution of n points per unit length of the smallest eddy, the total number of mesh points required will scale with $n \cdot Re^{\frac{9}{4}}$. Integrate in time the NSF with a time step determined by the smallest turbulent time scales, which is proportional to $Re^{\frac{3}{4}}$, the total computational effort is proportional to Re^3 for homogeneous turbulence! Considering an industrial application where realistic Reynolds numbers are of the order of 10^5 - 10^7 , the computational time is very expensive.

3.2. Large Eddy Simulation (LES)

The equations are obtained from the NS conservation laws by filtering the part of the spectrum that is over the smaller length scales. Here the equations are averaged, the lowest identified scales are related to the mesh size and therefore the LES models are often referred to as subgrid scale models. The large-scale turbulent fluctuations are directly simulated and the computational requirements are still very high. The same reasoning can be done here; the total computational effort is proportional to $Re^{\frac{9}{4}}$, lower than DNS but still excessively high for large Reynolds applications particularly for wall-bounded flows.

3.3. Reynolds Averaged Navier-Stokes Equations (RANS)

For the most industrial applications, the approximation of Reynolds Averaged Navier-Stokes equations averaged the turbulent equations, in time, over the whole spectrum of turbulent fluctuations. This requires, in additions, empirical or semi-empirical information on the turbulence structure and its relation to the averaged flow. The time averaging has to remove the dependency of the turbulent fluctuations, without destroying the time dependence connected with other time-dependent phenomena with other time scales.

For any turbulent quantity A, the separation

$$A = \bar{A} + A' \quad (3.1)$$

Is introduced with

$$\bar{A}(x, t) = \frac{1}{T} \cdot \int_{-\frac{T}{2}}^{+\frac{T}{2}} A(x, t + \tau) d\tau \quad (3.2)$$

\bar{A} represents a time-averaged turbulent quantity, where T is to be chosen large enough compared with the time scale of the turbulence but small enough compared with the time scales of all other unsteady phenomena. A' is the turbulent fluctuating part, which is of stochastic nature.

Applying the averaging at the momentum equation is possible to find the Reynolds stresses, added to the averaged viscous shear stresses. The relation between Reynolds stresses and the mean flow quantities are unknown. Therefore, other models based on theoretical consideration are required. None of the available turbulence models offers a totally accurate description of turbulent flows and although the RANS approximations is the most widely used in practice, the turbulent model components are their weakest link.

Since the RANS approximations are the most used, their application for turbulent flow will be treated in the following chapter, where the turbulence models will be described.

4. Basic discretization techniques

The computer cannot solve the Navier-Stokes equations analytically, so the main objective now is to choose correctly the discretization of the mathematical model. The discretization involves two components, the space discretization and the equation discretization.

The space discretization consists in setting up a mesh, or a grid, by which the continuum of space is replaced by a finite number of point where the numerical values of the variables will have to be determined. It is obvious that the accuracy of the solution is proportional to the refinement of the mesh. In addition, the quality of the mesh is important, so it is essential to define a good mesh.

The second component is the equation discretization; the equation can be discretized involving the values of the unknowns related to the mesh point. The basis of all numerical methods consists in this transformation of the mathematical model into an algebraic, linear or nonlinear, system of equations for the mesh-related unknown quantities.

There are three families of methods for space derivatives:

- Finite difference method (FDM), reference for all studies of numerical discretization, only applicable to structured grid;
- Finite volume method (FVM), which discretizes directly the integral form of the conservation laws. It is general, simple, easy to applicate to both structured and unstructured grid;
- Finite element method (FEM), derived from structural mechanics, but not exclusively applied in CFD world (not treated in this chapter).

4.1. Finite difference method (FDM)

The oldest method applied to obtain numerical solution, the idea of finite difference is simple, because it corresponds to an estimation of derivative by ratio of two differences according to theoretical definition of the derivative.

For a function $u(x)$ the derivative point x is defined by:

$$u_x = \frac{\partial u}{\partial x} = \lim_{\Delta x \rightarrow 0} \frac{u(x + \Delta x) - u(x)}{\Delta x} \quad (4.1)$$

The expression approximates the exact value of u_x , all depends on how much delta x is small. It introduces a truncation error, which goes to zero for delta x tending to zero. The power of delta x , with which this error tends to zero, is called “order of accuracy of difference approximation”, and can be obtained from Taylor series development of $u(x + dx)$ around x .

$$(u_x)_i = \left(\frac{\partial u}{\partial x}\right)_i = \frac{u_{i+1} - u_i}{\Delta x} - \frac{\Delta x}{2} (u_{xx})_i - \frac{\Delta x^2}{6} (u_{xxx})_i + \dots = \frac{u_{i+1} - u_i}{\Delta x} + O(\Delta x) \quad (4.2)$$

This series is called first order forward difference, if replacing dx with $-dx$ it is possible to obtain the first order backward difference. Combine this two difference that involves the points to the left and to the right of point i , lead to a central difference formula.

$$(u_x)_i = \frac{u_{i+1} - u_{i-1}}{2\Delta x} - \frac{\Delta x^2}{6} (u_{xxx})_i + \dots = \frac{u_{i+1} - u_{i-1}}{2\Delta x} + O(\Delta x^2) \quad (4.3)$$

The figure below shows the geometrical difference between all difference formula.

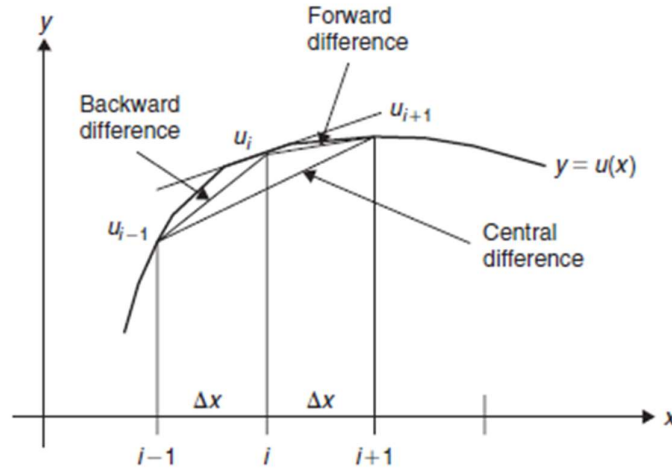


Figure 4.1 Geometrical meaning between the difference formula.

If higher order derivatives is required, it can be obtained repeating the first order formula

$$(u_x)_i = \left(\frac{\partial^2 u}{\partial x^2}\right)_i = \frac{(u_x)_{i+1} - (u_x)_i}{\Delta x} = \frac{u_{i+1} - 2u_i + u_{i-1}}{\Delta x^2} + O(\Delta x^2) \quad (4.4)$$

A simple observation can be done looking at all the formula: any difference equation, for any order of derivative and in any number of dimensions, must always satisfy the condition that the sum of its coefficients is equal to zero.

Applying difference methods to linear one dimensional convection equation is simple, using the formula described before. The discretization of space and the discretization of time must be done separately. Indicated the time level n by a superscript and the space position by the subscript i , the time axis is subdivided in constant time intervals Δt with (see figure 4.2):

$$x_i = i\Delta x \quad t^n = n\Delta t \quad (4.5)$$

$$u_i^n = u(i\Delta x, n\Delta t) \quad (4.6)$$

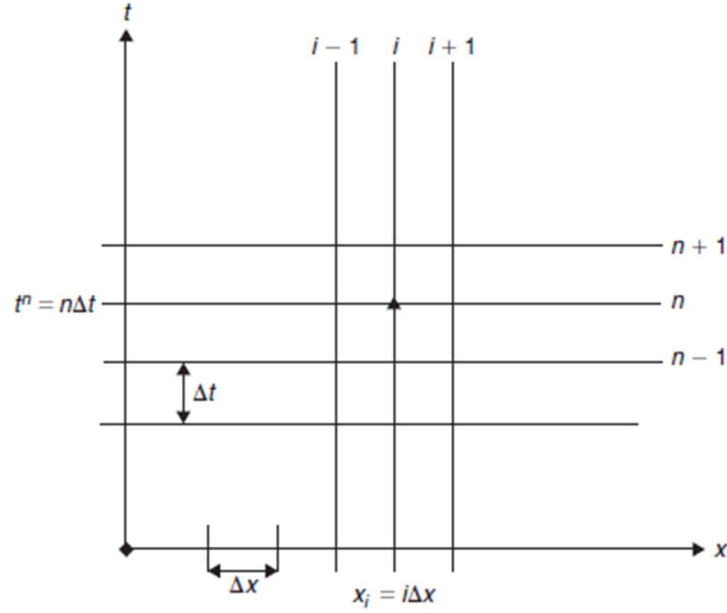


Figure 4.2 Discretization of the time and the space axis.

Applying the formula of central space derivative to point i leads to the semi-discrete scheme, called method of lines:

$$(u_t)_i = -\frac{a}{(2\Delta x)}(u_{i+1} - u_{i-1}) \quad (4.7)$$

After that, the next step is to define the a discretization time, it is logical take forward difference formula of the time, leading to

$$\frac{u_i^{n+1} - u_i^n}{\Delta t} = -\frac{a}{(2\Delta x)}(u_{i+1} - u_{i-1}) \quad (4.8)$$

This method is known as the Euler method for the time integration of ordinary differential equations, leading to the explicit numerical scheme:

$$\frac{u_i^{n+1} - u_i^n}{\Delta t} + \frac{a}{(2\Delta x)}(u_{i+1}^n - u_{i-1}^n) = 0 \quad (4.9)$$

The very economical in terms of number of arithmetic operations necessary for progressing in time, is in contrast with the restriction on time step Δt , which has to be quite short for stability conditions. Instead evaluating the $(n + 1)$ level, leads to the implicit scheme:

$$\frac{u_i^{n+1} - u_i^n}{\Delta t} + \frac{a}{(2\Delta x)}(u_{i+1}^{n+1} - u_{i-1}^{n+1}) = 0 \quad (4.10)$$

Known as backward or implicit Euler method. Instead of using a central difference discretization for space, it is possible to use a backward difference in space. After the semi-discrete in space, as before, the time can be discretized for explicit and implicit schemes, leading to:

$$\frac{u_i^{n+1} - u_i^n}{\Delta t} + \frac{a}{(2\Delta x)}(u_i^n - u_{i-1}^n) = 0 \quad (4.11)$$

These schemes are first order in space and in time and are known as the first order upwind schemes for the convection equation.

Considering the diffusion equation, the discretization is second order in space and first order in time, and again choosing the implicit or explicit scheme leads to

$$\frac{u_i^{n+1} - u_i^n}{\Delta t} + \frac{a}{(2\Delta x)} (u_i^n - u_{i-1}^n) = 0 \quad (4.12)$$

$$\frac{u_i^{n+1} - u_i^n}{\Delta t} + \frac{a}{(2\Delta x)} (u_i^{n+1} - u_{i-1}^{n+1}) = 0 \quad (4.13)$$

Taking the average of these two schemes, a well-known scheme for this parabolic time-dependent diffusion equation can be obtained, leading to the Crank-Nicholson scheme:

$$u_i^{n+1} = u_i^n + \frac{1}{2} \frac{\alpha \Delta t}{\Delta x^2} (u_{i+1}^{n+1} - 2u_i^{n+1} + u_{i-1}^{n+1}) + \frac{1}{2} \frac{\alpha \Delta t}{\Delta x^2} (u_{i+1}^n - 2u_i^n + u_{i-1}^n) \quad (4.14)$$

This scheme is second order in time and in space.

This method is good for uniform mesh, for non-uniform grid (like grids on boundary layers region), the thickness changes like the inverse of the square root of the Reynolds number. If the aim is to ensure that the velocity variations in the x - and y - directions are of the same order, it should generate a grid with an aspect ratio $\frac{\partial x}{\partial y}$ of the order of

$$\frac{\partial x}{\partial y} \sim \frac{1}{\sqrt{Re_x}} \quad (4.15)$$

This leads to a rather small and unrealistic cell for realistic number of Reynold, so the accuracy can be low. Therefore, the differences formulas generally can lose at least one order of accuracy, and sometimes two, on general non-uniform grids.

4.2. Finite Volume Method (FVM)

The finite volume method is based on cell-averaged values; the main numerical quantities are the local function values at the mesh points. The advantage of FVM is that the conservative discretization is automatically satisfied, through the direct discretization of the integral form of the conservation law.

Taking a general conservation law like:

$$\frac{\partial}{\partial t} \int_{\Omega} U d\Omega + \oint_S \vec{F} \cdot d\vec{S} = \int_{\Omega} Q d\Omega \quad (4.16)$$

The scalar value U inside the volume only depends on the surface values of the fluxes. Supposed to divide the internal volume in subvolume, it is possible to see an interesting property: the contributions of the internal lines always appear twice but with opposite signs. This property has to be satisfied by the numerical discretization of the flux contributions in order for a scheme to be conservative. If this is not the discretization, it is said to be non-conservative, the internal flux contributions appear as numerical internal volume sources.

For one-dimensional form of the conservation law:

$$\frac{\partial u}{\partial t} + \frac{\partial f}{\partial x} = q \quad (4.17)$$

With f is the flux x -component vector. A central difference applied to a finite volume mesh the discretized equation is obtained at point $(i \pm 1/2)$ of the figure 4.3, assuming constant cell sizes:

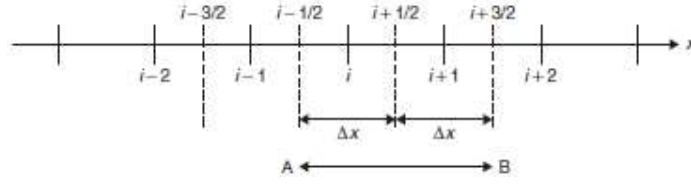


Figure 4.3 Subdivision of a one-dimensional space into mesh cells

$$\frac{\partial u_i}{\partial t} + \frac{f_{i+1/2} - f_{i-1/2}}{\Delta x} = q_i \quad (4.17)$$

The same discretization applied to the point $(i + 1)$ and $(i - 1)$, will give

$$\frac{\partial u_{i+1}}{\partial t} + \frac{f_{i+3/2} - f_{i+1/2}}{\Delta x} = q_{i+1} \quad (4.18)$$

$$\frac{\partial u_{i-1}}{\partial t} + \frac{f_{i-1/2} - f_{i-3/2}}{\Delta x} = q_{i-1} \quad (4.19)$$

The sum of these three equations is a consistent discretization of the conservation law for the cell AB

$$\frac{\partial}{\partial t} \left(\frac{u_i + u_{i+1} + u_{i-1}}{3} \right) + \frac{f_{i+3/2} - f_{i-3/2}}{3\Delta x} = \frac{q_i + q_{i-1} + q_{i+1}}{3} \quad (4.20)$$

The same thinking can be done for non-conservative equation. The result that is obtained is the same with the difference that internal sources rise in the equation.

As said before the strength of the FVM is its direct connection to the physical flow properties. The basis of the method relies on the direct discretization of the integral form of the conservation law. This is different from FDM, it discretize the differential form of the conservative laws. The FVM requires setting up the following steps:

- Subdivide the mesh, obtained from the space discretization, into finite volumes, one control volume being associated to each mesh point.
- Apply the integral conservation law to each of these finite volumes.

When adding the contributions of the neighbouring finite volumes, the consistency of a valid discretization does not have to be lost. For this purpose it is important evaluate the relation between the control volumes and the grid, following two different approaches:

- A cell-centered approach, the unknowns are at the centres of the mesh cells and the grid lines define the finite volumes and surfaces.
- A cell-vertex approach where the unknowns are defined at the corners of the mesh.

The control volumes must follow some constraints for a consistent finite volume method:

- i. Their sum should cover the entire domain.
- ii. The subdomains are allowed to overlap with the conditions that each part of the surface appears as part of an even number of different subdomains such that the overall integral conservation law holds for any combination of the adjacent subdomains.
- iii. Fluxes along cell surface have to be computed by formulas independent of the cell in which they are considered.

The last constraint ensures that the conservative property is satisfied.

In short, the main difference between FDM and FVM is that the first is a discretization of the differential equation (local description of the physical properties); the last is a discretization of the integral equation (applied to the entire fluid domain). Moreover, the FDM can have a low

accuracy for non-uniform grid mesh; the FVM, with the right formulas, can easily describe the surface and volume cells with an acceptable accuracy.

4.3. Mesh generation

As said in previous paragraph, the most common method used for discretization in CFD application is the Finite Volume Method (FVM). The first step for setting up a CFD simulation is to analyse the geometry (complex in most applications), and discretize the fluid domain that concern. The application treated on this work is a problem of internal fluid dynamics; the fluid domain is constrained to pass through different ducts. Moreover, the simulation examines interaction between fluid and complex internal geometry, for the purpose of swirl the fluid to obtain a good mixing of the flow. It is easy to understand in this application how well has to be made the mesh if it is desired a good level of accuracy. However, the equations of fluid dynamics are computed in every single control volume that form the fluid domain, if in one side the accuracy depends on how refined is the mesh size, in the other the time for generating a fine mesh and the simulation time could be rather high. Need to reach a compromise but with a good level of accuracy, this could be made following a convergence method. It is useful to ensure that the results do not depend on the mesh size. Another method to understand if a simulation can converge is to match the experimental results with simulation results. This is not always simple because the nature of the two data can be different, in addition, the experimental data could be affected by errors, or the CFD simulation could be not accurate if the residuals are high or not converge.

Having said that, there are some expedients for avoid low accuracy results, or expensive computational time. Generating a good mesh following these expedients means to understand what actually happens in the flow field. For instance, if an uniform flow is expected, a wider cell size can be generate, instead, where the geometry is more complex and high turbulence fluid flow are expected, finer cells size is required for better catch the gradient of velocity. Furthermore, care must be taken when discretize the boundary layer. Here no-slip condition is assumed, and the boundary layer must be solved using very thin cells. This type of mesh is called *prism layers* mesh and in a manner of speaking, they represent the discretization of the boundary layer. These cells are thin enough for better catch the velocity gradients in the normal direction with respect to the wall. The *core mesh* is the discretization that start from the last cell of these layers.

Boundary layer has a wide range of application especially in aerodynamics, for example useful to determine the drag coefficient, or in heat transfer problem where the purpose of the simulation is to determine the heat transfer coefficient. In a point of view of mesh generation, the prism layers becomes important because at high Reynolds number, the viscous sublayer of a boundary layer is so thin that it is difficult to use enough grid points to resolve it. This problem can be avoided by using *wall functions*, which rely on the existence of a logarithmic region in the velocity profile. Looking the figure below:

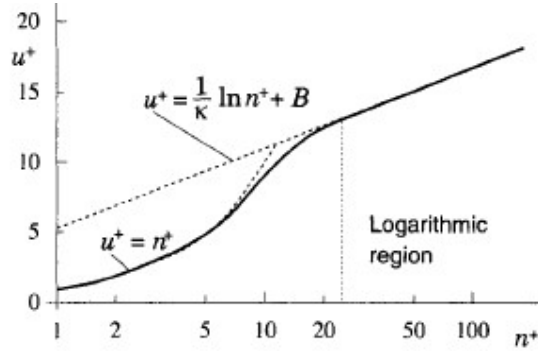


Figure 4.4 Wall function (n^+ is equal to y^+)

The velocity profile, relates the non-dimensional velocity with the non-dimensional distance from the wall. The y^+ is defined as:

$$y^+ = \frac{y u_t}{\nu} \quad (4.21)$$

Where u_t is the friction velocity and y is the distance from the wall. The friction velocity is defined as:

$$u_t = \sqrt{\left(\frac{t_w}{\rho}\right)} \quad (4.22)$$

The wall non-dimensional velocity u^+ is defined as:

$$u^+ = \frac{u}{u_t} \quad (4.23)$$

The empirical law that correlate these two non-dimensional values is expressed by the law of the wall, in particular the following relation is assumed:

$$u^+ = \begin{cases} y^+ & \text{if } y^+ < 5 : \text{viscous sublayer} \\ \frac{1}{k} \log y^+ + c & \text{if } y^+ > 50 : \text{log region} \end{cases} \quad (4.21)$$

Where $k = 0.41$ is called the von Karman constant and $c = 5.5$ is an empirical constant related to the thickness of the viscous sublayer (this value of c is obtained for smooth flat plate; for rough walls, smaller values are obtained). If $y^+ < 5$, the velocity profile is linear and the viscous stresses are dominant. The relation is logarithmic in the log region for $y^+ > 50$. The range $5 < y^+ < 30$ is where the buffer layer is located, the shear and viscous stresses are comparable with each other.

The value of y^+ can be set choosing the thickness of the first prism layer. The y^+ has to be monitored during simulation because the turbulence model chosen depends on its value. This will be explained in the next chapter where the most used turbulence models will be described. Generally, there are some turbulence model that required staying in a lower range of y^+ ; others are good for higher range. The wall function above described are implemented in the software STAR CCM+ in order to take into account the effects of the viscous sublayer. It is good practice not to fall in the buffer layer, since it is a transitional region and the solution can be less accurate.

In conclusion, in **STAR CCM+** is possible to choose different volume cells type. It is good to choose the type that fills better the fluid domain. The different types of the core mesh that can be set are:

- *Polyhedral cells*: provide a balanced solution for complex mesh generation problems. Easy and efficient to build, contain approximately five times fewer cells than a tetrahedral mesh for a given starting surface. The high level of accuracy that they provide is contrasted with the time spent to generate the mesh.
- *Tetrahedral cells*: is the fastest and uses the least amount of memory for a given number of cells. The quality of the surface mesh must be good to ensure a good quality volume mesh because the it is strictly conforms to the triangulation of the surface at the domain boundary.
- *Trimmed cells*: provides a robust and efficient method of producing a high-quality grid for both simple and complex mesh generation problem. The accuracy is lower than polyhedral cells but the time spent to generate this mesh is less. This kind of mesh is more used for external applications.
- *Thin cells*: generate a prismatic type volume mesh for thin volumes within parts or regions. Thick or bulk portions of the same geometry are meshed with the core volume mesh. It is typically used for thin plate geometries, where good quality cells are required to capture the solid material thickness adequately (useful for heat transfer analysis).

5. Turbulence models

The Reynolds number of a flow gives a measure of the relative importance of inertia forces and viscous forces. Turbulent flows are highly unsteady and the velocity would appear random. It is cause of great dissipation; the kinetic energy is irreversibly converted in internal energy of the fluid. The great vortexes increase the intensity of turbulence. These are also responsible for the stirring of fluid; parcels of fluid with different concentrations are brought into contact generating the process called turbulent diffusion. Create turbulence in particular points of the fluid flow is wanted in many applications.

Cause of these complex properties of the turbulence phenomena, it is not simple write an equation that can predict perfectly the velocity profile. Fortunately, the engineers are interested in knowing few quantitative properties of the turbulent flow and in RANS approach all of the unsteadiness is average out. Need to start from the Reynolds decomposition seen before and apply to continuity equation and momentum conservation equation. From eq. (3.1) and (3.2), the corresponding density-weighted average is defined through

$$\tilde{A} = \frac{\overline{\rho A}}{\bar{\rho}} \quad (5.1)$$

With

$$A = \tilde{A} + A'' \quad (5.2)$$

And

$$\overline{\rho A''} = 0 \quad (5.3)$$

The averaged continuity equation becomes

$$\frac{\partial}{\partial t} \bar{\rho} + \bar{\nabla} \cdot (\bar{\rho} \vec{v}) = 0 \quad (5.4)$$

The averaged momentum equations lead to the Reynolds stress tensor. All variables are considered as averaged quantities (density and pressure as time averages and velocities as density-weighted averages):

$$\frac{\partial}{\partial t} (\bar{\rho} \vec{v}) + \bar{\nabla} \cdot (\bar{\rho} \vec{v} \otimes \vec{v} + \bar{p} \bar{I} - \bar{\tau}^v - \bar{\tau}^R) = 0 \quad (5.5)$$

With the Reynold stresses $\bar{\tau}^R$ defined by

$$\bar{\tau}^R = -\overline{\rho v_i'' \otimes v_j''} \quad (5.6)$$

In Cartesian coordinates

$$\tau_{ij}^R = -\overline{\rho v_i'' v_j''} \quad (5.7)$$

Where \vec{v}'' designates the turbulent fluctuating velocity vector. Also the mean turbulent total energy can be defined by the following relation, the overbar indicates the time average,

$$\bar{\rho} \tilde{E} = \bar{\rho} \bar{E} = \overline{\rho \left(e + \frac{\vec{v}^2}{2} \right)} \quad (5.8)$$

We obtain

$$\tilde{E} = \bar{e} + \bar{k} + k = \hat{E} + k \quad (5.9)$$

Where \tilde{k} is the kinetic energy of the mean flow per unit mass

$$\bar{\rho}\tilde{k} = \bar{\rho}\frac{\overline{\tilde{v}^2}}{2} \quad (5.10)$$

And k is the turbulent kinetic energy; thus

$$\bar{\rho}k = \rho\frac{\overline{\tilde{v}^2}}{2} = \overline{\rho k''} \quad (5.11)$$

It is defined as the average of the kinetic energy k'' of the turbulent fluctuations.

The averaged procedure has produced the Reynolds stress term but this quantity is unknown, in particular its relation to the mean flow variables, so need to model this relation, based on theoretical consideration coupled to the unavoidable empirical information. This information is considered to be contained in the turbulence models, to be added to the averaged Navier-Stokes equations. The most used turbulence models are the k epsilon model that is a two-equation model. The other model is the k omega model, another two equations model. The first is the most popular model in industrial application, instead the second is the main rival of k epsilon model. These will be described in the following paragraph.

5.1. The k-epsilon model

This model is based on transport equations for the kinetic energy of the turbulence k and for the turbulent dissipation epsilon.

The various models rely on the Prandtl-Kolmogorov expression

$$\nu_T = C_\nu k^{1/2} L \quad (5.12)$$

Where $k^{1/2}$ and L act as representative velocity and the length scales of the turbulence. The dissipation ϵ can be written as

$$\epsilon = C_\epsilon \frac{k^{3/2}}{L} \quad (5.13)$$

And the turbulence viscosity as:

$$\nu_T = C_\mu \frac{k^2}{\epsilon} = \frac{\mu_T}{\bar{\rho}} \quad (5.14)$$

The structure of this equation has the general form of a transport equation. Modelling the equation of k , lead to this expression for the kinetic turbulence energy:

$$\frac{\partial}{\partial t}(\bar{\rho}k) + \vec{\nabla} \cdot (\bar{\rho}k\vec{v}) = \vec{\nabla} \cdot (\mu_k \vec{\nabla}k) + (\bar{\tau}^R \cdot \vec{\nabla}) \cdot \vec{v} - \bar{\rho}\epsilon + Q_k \quad (5.15)$$

The first term on the right hand side is a diffusion term, the second term denoted by P , is the production of turbulent energy by the work of the mass flow against the Reynold stresses τ^R . the third term is the dissipation contribution.

A similar equation can be assumed for the dissipation epsilon

$$\frac{\partial}{\partial t}(\bar{\rho}\epsilon) + \vec{\nabla} \cdot (\bar{\rho}\epsilon\vec{v}) = \vec{\nabla} \cdot (\mu_\epsilon \vec{\nabla}\epsilon) + C_{\epsilon 1} P \frac{\epsilon}{k} - C_{\epsilon 2} \bar{\rho} \frac{\epsilon^2}{k} f_2 + Q_\epsilon \quad (5.16)$$

Where P is the production term of the K equation. The terms Q_k and Q_e are additional terms introduced for specific flow situation. In the standard k- ϵ model both are equal to zero.

The eddy diffusivities μ_k and μ_ϵ associated with the kinetic energy and dissipation equations respectively are defined by:

$$\mu_k = \mu + \frac{\mu_T}{\sigma_k} \quad (5.17)$$

$$\mu_\varepsilon = \mu + \frac{\mu_T}{\sigma_\varepsilon} \quad (5.18)$$

The five constants have to be defined empirically. Typical values valid for a wide range of applications are shown on figure below

$$\begin{array}{lll} C_\mu = 0.09 & C_{\varepsilon 1} = 1.45 - 1.55 & C_{\varepsilon 2} = 1.92 - 2.00 \\ f_2 = 1 & \sigma_k = 1 & \sigma_\varepsilon = 1.3 \end{array}$$

Figure 5.1 Constant value of k-ε model

This model is able to predict complex flows such as separated and three-dimensional flows, and present an acceptable compromise between economy of calculations and accuracy of the results. These two equations are relatively simple to implement to a CFD code, during the simulation the equations have to be discretized and solved with the other equations. It was shown that the k-epsilon model is a good model for regions where the flow is fully turbulent, where there are not-separation of fluid and with light pressure gradient. Its main weakness is the numerical stiffness when equations are integrated through the viscous sublayer, which are treated with functions that have stability issues.

Anyway the computational cost is quite inexpensive compared with other models.

5.2. The k-ω model

Another two-equation model is the k-ω model. It uses the turbulent kinetic energy equation but it has to be modified a bit:

$$\frac{\partial(\rho k)}{\partial t} + \frac{\partial(\rho \bar{u}_j k)}{\partial x_j} = P_k - \rho \beta^* k \omega + \frac{\partial}{\partial x_j} \left[\left(\mu + \frac{\mu_t}{\sigma_k^*} \right) \frac{\partial \omega}{\partial x_j} \right] \quad (5.19)$$

The same things said above can be applied here. The ω equation as given by Wilcox (1998) is:

$$\frac{\partial(\rho \omega)}{\partial t} + \frac{\partial(\rho \bar{u}_j \omega)}{\partial x_j} = \alpha \frac{\omega}{k} P_k - \rho \beta \omega^2 + \frac{\partial}{\partial x_j} \left[\left(\mu + \frac{\mu_t}{\sigma_\omega^*} \right) \frac{\partial \omega}{\partial x_j} \right] \quad (5.20)$$

The eddy viscosity is expressed as

$$\mu_t = \rho \frac{k}{\omega} \quad (5.17)$$

The coefficients that go into this model are a bit more complicated than those in the k-epsilon model. They are:

$$\alpha = \frac{5}{9}, \quad \beta = 0.075, \quad \beta^* = 0.09, \quad \sigma_k^* = \sigma_\omega^* = 2, \quad \varepsilon = \beta^* \omega k$$

Figure 5.2 Constant values k-ω model

The numerical behaviour of this model is similar to that of the k-ε, but it allows a more accurate near wall treatment with an automatic switch from a wall function to a low-Reynolds number formulation based on grid spacing. It demonstrates superior performance for wall-bounded and low Reynolds number flows. Shows potential for predicting transition. It performs

better under adverse pressure gradient condition, but the separation is typically predicted to be excessive and early. For this reason, it requires a mesh resolution near the wall.

A variant of the standard k - ω model is the Shear Stress Transport (SST), it combines the original k - ω for use near walls and the standard k - ϵ model away from walls using a blending function, and the eddy viscosity formulation is modified to account for the transport effects of the principle turbulent shear stress. This model may be more appropriate for separated flows.

6. Lagrangian Multiphase Flow

Multiphase flows are found in a wide variety of industrial processes like internal combustion engines, spray, chemical reactors etc. A flow is multiphase when it comprehends more than one phase, not only the chemical definition of phase (gas, liquid or solid) but also the diameter classes or a broad distribution of states (such as temperature). All these processes can be easily described by the Lagrangian multiphase model, this model in particular simulate and track the flow path of dispersed particles in a continuous phase including the associated heat and mass transfer phenomena such as droplet evaporation. One task of the work done in this master thesis will be the particles injection of a Lagrangian phase inside the continuum flow. The Lagrangian multiphase and all the others models used for simulate the particles injection will be described in the following paragraphs.

The Lagrangian numerical methods can be used in conjunction with Eulerian numerical methods to describe these situations where individual particle dynamics impact the solution on the scale that is resolved in the Eulerian field. A Lagrangian reference frame is used to describe the evolution of an individual particle and the equations of change are written following it. If particles are released to a turbulent carrier flow, each of them has their own random path due to interaction with the fluctuating turbulent velocity field. If the dispersed phase evaporate, mass transfer occurs between the phases, with others effects like heat transfer. The collisions between particles can produce two different effects that are cause of the size changing of particles: break up into smaller particles or agglomeration into bigger particles. The boundary condition at wall can determine the behaviour of the particles when they hit wall.

STAR CCM+ distinguishes between different types of particles: material, massless, multicomponent and DEM (discrete element method). The phase that will be described and used for the following analysis is the material particles that is the most general Lagrangian multiphase dispersed phase. The particles have mass and volume and are governed by the Lagrangian conservation laws of mass, momentum and energy.

The conservation equation of momentum for a particle is written in Lagrangian framework. The change in momentum is balanced by surface and body forces that act on the particle. The equation of conservation of momentum for a material particle of mass m_p is given by:

$$m_p \frac{dv_p}{dt} = F_S + F_B \quad (6.1)$$

Where v_p is the instantaneous particle velocity, F_S is the resultant of the forces that act on the surface of the particle, and F_B is the resultant of the body forces. They can be written as:

$$F_S = F_d + F_p + F_{vm} \quad (6.2)$$

$$F_B = F_g + F_{MFR} + F_u + F:c + F_{Co} \quad (6.3)$$

Where

- $F_d \rightarrow$ drag force
- $F_p \rightarrow$ gradient pressure force
- $F_{vm} \rightarrow$ virtual mass force
- $F_g \rightarrow$ gravity force
- $F_u \rightarrow$ user defined force
- $F_c \rightarrow$ contact force (only DEM)
- $F_{Co} \rightarrow$ Coulomb force

The F_s represents the momentum transfer from the continuous phase to the particle. With the two-way coupling modelling approach, F_s is accumulated over all the parcels and applied in the continuous phase momentum equation.

6.1. The Drag Force

The drag force is defined as:

$$F_d = \frac{1}{2} C_d \rho A_p |v_s| v_s \quad (6.3)$$

Where

- $C_d \rightarrow$ drag coefficient of the particle
- $\rho \rightarrow$ density of the continuous phase
- $v_s = v - v_p \rightarrow$ particle slip velocity and v the instantaneous velocity of the continuous phase
- $A_p \rightarrow$ projected area of the particle

The drag coefficient is a function of the small-scale flow features around the individual particles. These features are impractical to resolve spatially, so the usual practice is to obtain the drag coefficient from correlations deriving from experiment or theoretical studies.

6.2. Pressure Gradient Force

The pressure gradient force is defined as:

$$F_p = -V_p \nabla p_{static} \quad (6.4)$$

Where V_p is the volume of the particle and ∇p_{static} is the gradient of the static pressure in the continuous phase.

6.3. Particle Position and Velocity

The variables describing the state of the particle change as a function of the time and space due to the resultant of the forces. The particle position and particle velocity are obtained by numerically integrating over time the particle momentum equation and the position equation:

$$\frac{dr_p}{dt} = v_p \quad (6.5)$$

Where $r_p(t)$ is the instantaneous position vector. A particle trajectory is the locus of points obtained by the integration of the position equation. The particles, which have the same state and evolve at the same way, are grouped in parcels. The exchange with the Eulerian phase is multiplied by the number of particles that the parcel represents.

6.4. Turbulent Dispersion

A particle in turbulent flow follows a randomly-varying velocity field, in according to its inertia. This behaviour is modelled by a stochastic approach that includes the effect of instantaneous velocity fluctuations on the particle. The particle remains in the eddy until either the eddy time-scale is exceeded, or the separation between the particle and the eddy exceeds the length scale of the eddy. The instantaneous velocity of the particle is:

$$v = \bar{v} + v' \quad (6.6)$$

Where v' is the local Reynolds-averaged velocity and v'' is the eddy velocity fluctuation, unique to each particle.

6.5. Particle Mass Balance

The equation of conservation of mass of a material particle is given by:

$$\frac{dm_p}{dt} = \dot{m}_p \quad (6.7)$$

Where m_p is the mass of the particle and \dot{m}_p the rate of mass transfer to the particle. The latter is zero unless mass transfer occurs, such as evaporation. With the two-way coupling model the rate of mass \dot{m}_p is accumulated over all the parcels and applied in the continuous phase continuity equation.

6.6. Droplet Evaporation

Quasi-steady single-component droplet evaporation assumes droplets to be internally homogeneous, consisting of a single liquid component. The rate of change of droplet mass due to quasi-steady evaporation \dot{m}_p can be written as:

$$\dot{m}_p = -g^* A_S \ln(1 + B) \quad (6.8)$$

Where B is the Spalding transfer number and g^* is the mass transfer conductance (to be precise, in the limit $B \rightarrow 0$). There are implemented on model three modes of evaporation:

- Super – Critical (active when droplet temperature exceeds critical temperature).
- Heat Transfer Limited Evaporation (active when vapour at the droplet surface is saturated and subcritical. The evaporation rate results from the balance between heat transfer from the vapour and latent heat transfer due to evaporation).
- Vapour Diffusion Limited Evaporation (active when vapour at the droplet surface is subcritical and not saturated. The evaporation rate depends on the rate at which vapour can diffuse away from the droplet).

The condensation for this model is treated as “reverse evaporation”.

6.7. Two-Way Coupling with the Continuous Phase

This model simulate the interactions between the dispersed phase and the continuous phase, where the momentum, heat and mass are exchanged between the phases. The effects of the dispersed phase on the continuous phase such as displacement, interphase momentum, mass and heat transfer changes when the Lagrangian dispersed phase equations are integrated over a cell. The balance of all these changes for all the particles provides the net momentum, mass, and energy that is exchanged with the continuous phase. These enter in the continuous equations as source terms. For brevity the source terms here will be not shows but they can be easily obtain.

6.8. Particle Injection

The injectors are discrete locations where the particles enter in the fluid domain. They define the size and the velocity vector distribution of the particles, the frequency (for unsteady simulation), and the particle temperature and composition for heat and mass transfer effects.

6.9. Particle Size Distribution

The particles that are injected can have different sizes. The injector generate different range of particle sizes that statistically are represented by a particle size distribution. The density of the particles in function of their size defines this distribution. In **STAR CCM+** the distribution is quantified using a cumulative distribution function (CDF) that can be defined using internal functions implemented on the software, or by a file table with the statistical distribution of the particle size (as done to simulate the injection in this work).

Last models used for simulate a good injection are those that describe the spray modelling, or rather the models that describe the breakup of a continuous liquid into droplets. Indeed a lot of industrial processes turning quantities of liquid into vapour. One of this is the vaporization and atomization of the fuel in the internal combustion chamber, or the urea injection for knocking down the NO_x in the after treatment system.

6.10. TAB Breakup

The Taylor analogy breakup (TAB) model is based on Taylor's analogy, that represents a distorting droplet as a damped spring-mass system. It considers only the fundamental mode of oscillation of the droplet where displacement and velocity of the system correspond to representative distortion and rate of distortion quantities for the droplet. Reach a critical value, the parent particles are replaced with child particles whose diameter is chosen from a Rosin-Rammler distribution. New parcels can be created but the original parcels are retained, only the diameter of the particles changes.

6.11. Wall Impingement

The impact of particles on rigid solid surfaces produces a variety of effects. These effects depend on the size, the velocity, the material of the impacting particles and on the nature of the surface. A liquid droplet can stick, bounce, or splash. The liquid that is deposited on the wall can retain the droplet form or it can merge into a fluid film. The model implemented on **STAR CCM+** used for the simulation is the Bai-Gosman.

6.12. Bai-Gosman Wall Impingement

The Bai-Gosman model aims to predict the outcomes of liquid droplets impacting an impermeable boundary ("wall") or fluid film. There are six possible regimes, illustrated in the following figure:

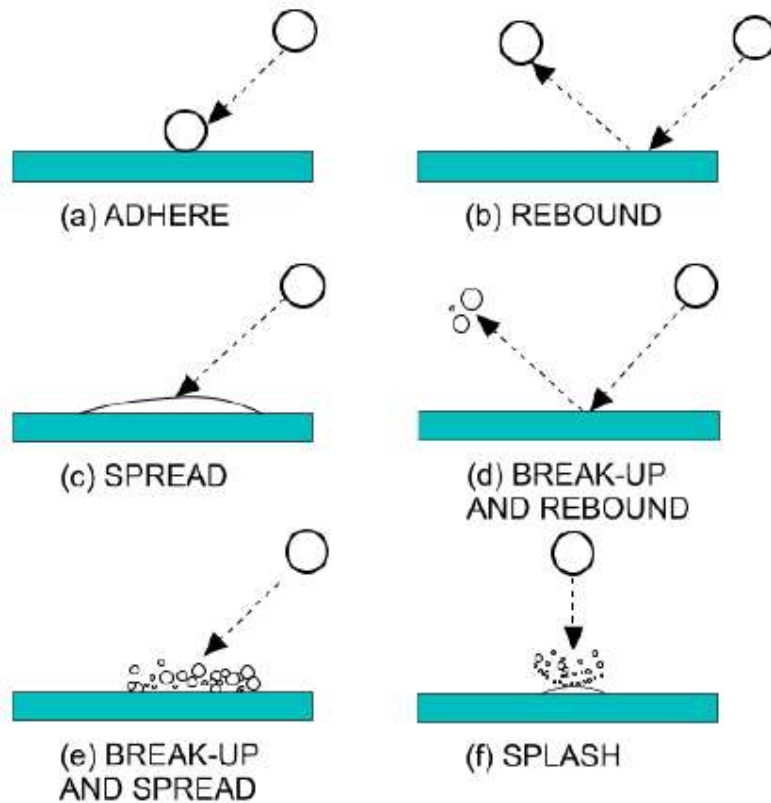


Figure 6.1 Bai-Gosman impingement condition

If the wall is a fluid film boundary, the film gains the momentum and kinetic energy lost by the droplets. The outcome of a liquid droplet after the impact on the wall depends on:

- Number of Weber;
- Wall temperature;
- The wall state.

The number of Weber is a dimensionless number that relate the inertia of the droplet and the surface tension. High number of Weber indicates that inertia is predominant, vice versa the surface tension is predominant. The number of Weber is plotted in function of the wall temperature. The zones are, for the dry state, thus separated:

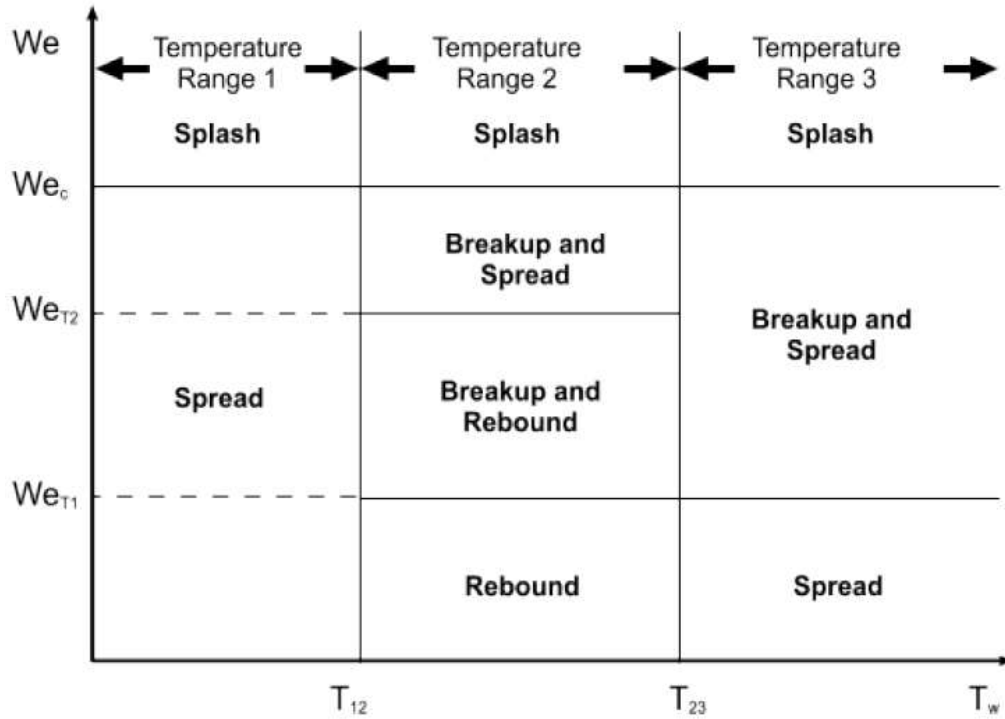


Figure 6.2 Zones impingement

Looking at this diagram it is possible to see that the different zones are divided based on particular number of Weber or particular range of temperature of the wall. The We_c is the limiting Weber number; its value can be calculated using the Laplace number with this relation:

$$We_c = ALa^{-0.18} \quad (6.9)$$

The T_{12} temperature range is expected to be approximately the boiling temperature of the droplet. The T_{23} temperature range is expected to be approximately the Leidenfrost temperature of the droplet. This value can be set on **STAR CCM+**, the chosen values will be explained when the moment will come. Also the We_{T_1} and We_{T_2} can be chosen, they are characteristic value for Weber number.

6.12.1. Parcel

To complete this chapter, here will be described how the particles are grouped into computational parcels that represent the total population of the dispersed phases. Each parcel represents a localized group (cluster) of dispersed phases having the same properties. Parcels are discretization of the population of dispersed phases in the same way that cells are a discretization of the continuous space. Their number is no arbitrary; it must be large enough so that the properties of the full population of dispersed phases are represented. It can be assessed by performing calculations with different numbers of parcels and comparing the results.

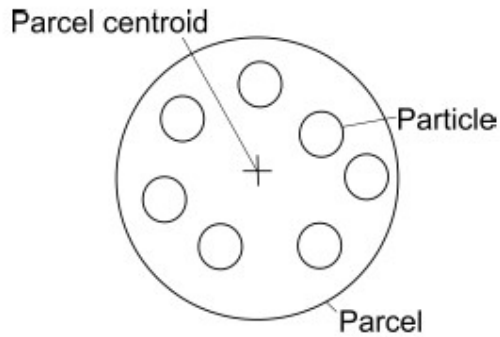


Figure 6.3 Parcel configuration

A parcel centroid determines the intersection of a Lagrangian parcel with a boundary face. The parcel centroid is the centre of mass of all the dispersed phases within the parcel.

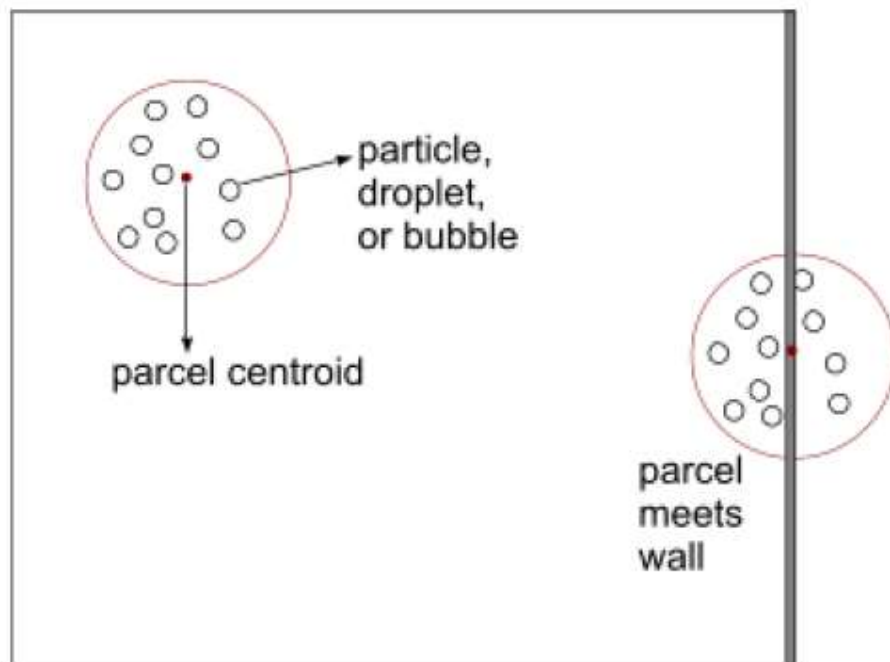


Figure 6.4 Parcel interaction with wall

STAR CCM+ does not provide the distribution of the dispersed phases in a parcel. The equation that rules the parcels are the same of that described for the particles. Within a parcel the particles do not interact with each other, but different parcels can breakup, bounce, collimate, coalesce.

As said in the previous paragraphs, momentum, mass, and energy of the particles are exchanged with the continuous phase. The number of parcels useful for the correct computing of the properties must be large enough, but remember that for each parcel, the equations in

Lagrangian frame are solved, so a compromise between accuracy and computation time has to be reached. Different boundary conditions can be made for the analysis of the dispersed phase into continuous phase; if particular condition are required, it is possible to choose for example to vaporize, to rebound or to escape the parcels at contact with the wall. Using escape condition, the parcels are deleted from the fluid domain and no more equations are solved for it.

7. After Treatment Systems

The formation of pollutants during combustion process in Diesel engine is strongly depending on non-uniformity of the charge, due to distribution of fuel variable in time. The substances that can be formed are HC, CO, NO_x and particulate. The presence of these harmful substances in the exhaust gas is serious for that application where the vehicle contribute to increase the pollution in urban areas.

The particulate and the NO_x are the main problems of the Diesel engine. It is important to adopt important measures for abatement of particulate and NO_x. Here will be explained only the formation of the NO_x and the technology that allows their reduction.

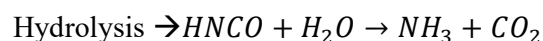
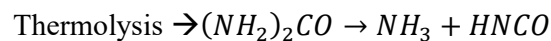
NO_x gases are usually produced by the reaction among nitrogen and oxygen during combustion of fuels; especially at high temperatures, such as occur in car engines. The NO_x is a generic term for the nitrogen oxides that are most relevant for air pollution, namely nitric oxide (NO) and nitrogen dioxide (NO₂). These gases contribute to the formation of smog and acid rain, as well as affecting tropospheric ozone. NO_x mainly formed through high temperature oxidation of the diatomic nitrogen found in combustion air. At high temperature, the nitrogen dissociate into their atomic states and participate in a series of reactions where the oxygen interact with it. Another mechanism of formation is the prompt, a mechanism of chain reaction promoted from the nitrogen atoms that react with radical CH present in the flame. At least another part of NO_x can derived from fuel. The nitrogen bonded to fuel, before entering in the zone of the flame, transform in radical the group CN that will be transform to NO in the zone of the flame.

There are different technologies that allows decreasing the pollution of NO_x. It is possible to act on cylinder for better improving the combustion and reduce the NO_x formation, but with an expensive cost for the calibration of the engine. There are other cheap systems capable to reduce the NO_x. Furthermore, with the growing pollution of the urban area, the normative became more pressing and the combination of these technologies for the after treatment of the gases is necessary.

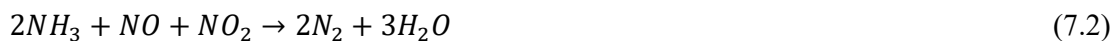
The more common systems use the catalysts capable to operate in minimal condition of consume. One of these is the SCR (Selective Catalytic Reduction).

7.1. Selective Catalytic Reduction (SCR)

The Selective Catalytic Reduction of the NO_x is a means of converting nitrogen oxides using a gaseous reductant, typically anhydrous ammonia, aqueous ammonia or urea; it is added to a stream of the exhaust gas and is adsorbed onto a catalyst. The SCR technology was already present in other applications like stationary diesel engine or industrial processes; successively it occurs in the automotive field. The SCR is possible for the selectivity of NH₃ to react with the nitrogen oxide to form N₂. It is a harmful gas; it must be stored and used in an organic compound called urea (CO(NH₂)₂). Commercially it is stored in a solution of water (32.5% urea 67.5 % water) called AdBlue. When injected the AdBlue evaporates and it splits by mean thermolysis and hydrolysis:



The NH₃ resultant is mixed with NO_x in exhaust gas, the reduction of NO_x occurs inside the monoliths:



The first reaction occurs rapidly and it is dominant without NO₂. With NO₂ there is an increase of the reduction activity, thanks to the second reaction that is also rapid. If the rate of $(NO_2)/NO > 1$ the dominant reaction is the third with a low reaction velocity.

The catalysts are made from various ceramic materials; active catalytic components are usually either oxides of base metals, or various precious metals. The most used are the catalysts made from base metals like vanadium, durability at high temperature is low but they are less expensive and work very well in a range of temperature most common in industrial application. Other materials used are the perovskite and the zeolites with reduced dimension and high efficiency at low temperature. The zeolites have more resistance at high temperature, so they are advantageous in that application where the regeneration occurs.

The conversion efficiency is very high (>90%) for SCR systems, they allow to calibrate the engine to minimum specific consume, and are reliable for long distance (>500000 km).

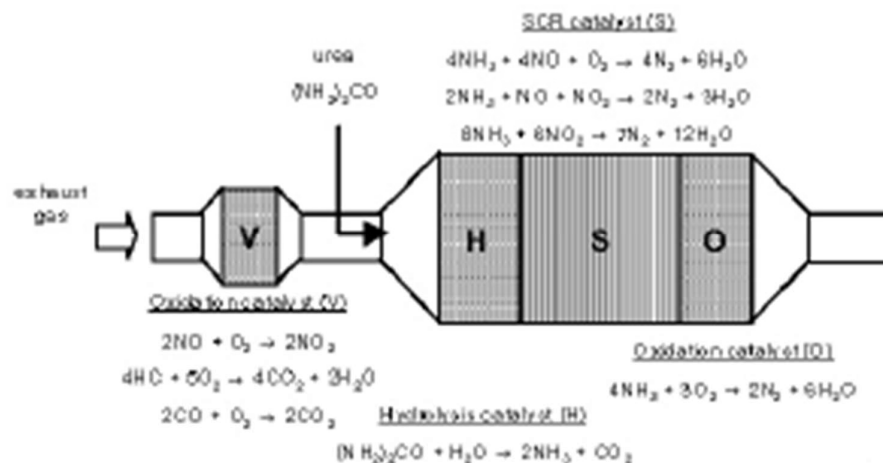


Figure 7.1 SCR scheme

- Looking at a figure of a SCR, the oxidation catalyst (V) is positioned before the reactor SCR for the oxidation of NO in NO₂ and optimize the rate of NO₂/NO, and speed the reaction. The hydrolysis catalyst (H) converts the solution of urea and water into NH₃ and CO₂, this component is optional because the SCR alone is capable to easily promote this reaction. The final oxidant catalyst (O) is necessary to clean-up eventual secondary emissions of NH₃ (ammonia slip) in dynamic work condition. Monitoring the concentration of NO_x is important to control the NH₃ quantity to inject. In order to do so, a NO_x sensor is positioned at the outlet of SCR that work good at low NO_x concentration (in a system in a non-functioning system, the high values of NO_x reduce the useful life of the sensor). The sensor placed at SCR outlet give an important

information to OBD (on board diagnostic), activating the closed loop control of the NH₃ quantity to be injected, limiting the ammonia slip.

The efficiency and the relative low cost of the SCR is in contrast with the multiple disadvantages:

- Necessity to implement the infrastructures for the transport and capillary distribution of the urea;
- The correct functioning depends on the utilizer which should provide to refuel the tank of urea on board;
- Larger dimensions required for the installation of the SCR system (not so critical in the sector of heavy transport);
- Ammonia slip
- Probability of formation of urea deposit inside the system.

To this list, it is possible to add the importance of reaching a good grade of mixing of NH₃ inside the SCR. Several studies have shown that the conversion efficiency of SCR go down if the NH₃ is not uniform. Moreover, the position of NO_x sensor is fundamental for a good reading of the concentration of NO_x. A bad measure is harmful for the correct functioning of the system; it could cause, for example, the last two point of the previous list.

The work of this master thesis attempts to analyse the position of the NO_x sensor by means CFD 3D in order to avoid the problems previously listed.

8. Passive Scalar Tracer method

In the previous chapters was described how to model the passive scalars. They basically are user-defined variables of arbitrary value, assigned to fluid phases or individual particle. They are passive because does not interact with the physical properties of the fluid domain. The best way to think of passive scalars is as tracer colour in a fluid but with the difference that they have numerical values instead of colour. The application of this method are various like:

- Choosing the best position for a sensor where there are multiple inlet pipes and only one outlet. With this method can be checked the discrete points in the computational domain that give the strongest signal of the passive scalar;
- Analysing the mixing of the two or more fluid stream with the same properties. Multiple passive scalars can be set to examine the effect of mixing;
- Tracing how smoke or any vapour would convect and diffuse in a room or any fluid domain. The dissolution of a gas in a liquid can be modelled.

The passive scalar is used in this master thesis to analyse the mixing of the gas exhaust at the SCR outlet. The hypothesis is to simulate how the NO_x leave the SCR and how much they are mixed when they reach the location of the NO_x sensor. This method is simply a way to simulate the mixing effect after the SCR outlet. It provides an indicator of the risk of locating a sensor in a bad location. In a real application the NO_x distribution at SCR outlet depends mainly on the distribution of the NH₃ at SCR inlet. How good or bad is the distribution, and how weak or strong is the mixing before reaching the sensor are the two factors that allow to evaluate if the sensor is doing its job or the values that it measures are bad.

The first simulations concern how the NO_x are mixed inside the fluid flow before reaching the sensor location. The distribution, as said, strongly depends on NH₃ distribution at SCR inlet, so need to think about which is the worst case to simulate in order to examine the mixing of NO_x. The idea is simple, the SCR outlet is subdivided in different sectors with the same area, and each one is initialised with a passive scalar. Here an example of the subdivision.

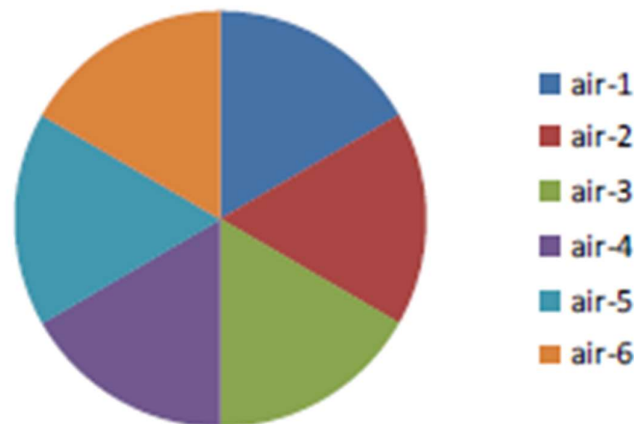


Figure 8.1 Subdivision of the section on six sectors

Each zone represent the worst scenario for the NO_x to pass through, all the other regions have no NO_x. Therefore, it is a binary distribution of the NO_x and the actual value of NO_x is independent from the source region. If it is supposed to have the section divided in 6, 8 or also 10 sectors, the mean value represents the target of mixing to reach in the sensor location for a

flow fully mixed downstream. It is possible to represent the distribution of the passive scalars using a mean deviation, for example, the mean deviation on SCR section for six passive scalars is defined as:

$$\bar{\delta} = \left(\left| 1 - \frac{1}{6} \right| \right) \cdot \frac{1}{6} + \left(\left| 0 - \frac{1}{6} \right| \right) \cdot \frac{5}{6} = 0.278 \quad (8.1)$$

Where in the first bracket there is the absolute deviation local to the tracer source, the value of the passive scalar is subtracted by the mean value of the passive scalar on the section, which is the target to reach (for 6 passive scalars, the mean value is $\frac{1}{6} = 0.1667$). The mean deviation is then normalised by the mean (target) value.

$$\text{norm. mean deviation} = \frac{\bar{\delta}}{\mu} = \frac{0.278}{0.1667} = 1.67 \quad (8.2)$$

Finally, the uniformity of the distribution can be defined as:

$$UI = 1 - \frac{1}{2} \left(\frac{\bar{\delta}}{\mu} \right) = 0.1667 \quad (8.3)$$

This demonstrates how the uniformity index is defined to represent the proportion of total section corresponding to a binary (something or nothing) distribution.

The value of one passive scalar at SCR section represents a hypothetical value of NOx [ppm], but it is only important to know what value it will become as a downstream target value when it becomes fully mixed. The figure below shows an example of input setting of passive scalars.

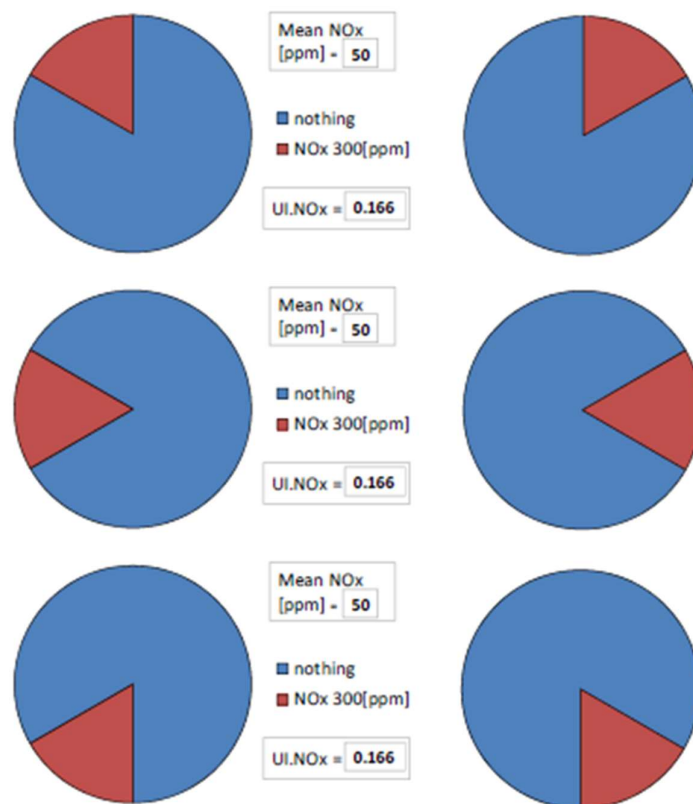


Figure 8.2 Example of input setting of passive scalars

The section is subdivided in six sector, each sector represents a concentration of NO_x, and the mean value represents, as said, the target to reach. The concentration of NO_x is considered fully mixed in downstream only if in the sensor location the value is equal to the target.

Instead of the real value of the NO_x, which is unknown, the concentration is represented with the passive scalar and initialised with value equal to one.

Post-processing the resulting mixture of any tracer by following the field of its scalar fraction, means finding the mixing response corresponding to a particular distribution with uniformity index = 1/6.

With this method, the post-processing of the six tracers can be done without restarting the simulation for every single passive scalar.

After giving a good explanation of this method and the logic of how it works, now it is necessary to understand which coefficient is the most appropriate to represent the grade of mixing in the different location. The mean deviation of the passive scalar normalized indicate how far the results are from the mean value (target). The logic of this coefficient is “lower is better”, this means that a low value of mean deviation indicate a high grade of mixing.

An intuitive way of thinking could be, for example, looking for a coefficient with a logic “higher is better”, which is a more appropriate manner to see the mixing of the NO_x along the fluid stream. This coefficient could be express as follow:

$$CoMix = \frac{\delta_{SCRout} - \delta_{Sensor}}{\delta_{SCRout}} \quad (8.4)$$

Where, the subtraction of the mean deviation (normalized or not, this is only a mathematical operation) computed on SCR outlet section and on sensor location, is related with the mean deviation on SCR outlet section. A high value should provide a high mixing of the flow on sensor location, vice versa this indicator says that the sensor could be in a bad position and could cause a failure of the urea injection control system. The target to respect are shows below:

CoMix < 60% Sensor will not read correctly
60% < CoMix < 70% Sensor could not read well
CoMix > 70% Sensor should read well

Figure 8.2 Mixing target

The first step of the simulation is to find a sensitivity of the passive scalars based on:

- Number of sectors in which the SCR outlet section is subdivided and consequently the number passive scalar used;
- Shape of passive scalars, instead of subdivide the section like pieces of pie, it is chosen to consider concentric circle always with the same area.

The second step was to evaluate the coefficient of mixing looking for example its value on:

- Surface that surrounds the sensor, which it takes into account of the mixing directly on the sensor.
- Volume that surrounds the sensor, a local volume around the sensor was taken into account for consider the mixing in the volume where the sensor should work rather than the surface only.

- Constraint surface that passes through the middle of the sensor, in this way the mixing was evaluated on all the pipe section.

In addition to coefficient of mixing, the uniformity index of every passive scalar was evaluated on the surface of the sensor and on the constraint section that pass through the section, then the mean value was computed. This index describes the distribution of the passive scalar on surface sensor or on constraint surface. High values of uniformity indicate that the quantity is distribute equally on surface, otherwise there will be zones where the sensor could read a distribution, and so a concentration, of NO_x that is wrong.

In the following paragraphs will be described the analysis done, the settings of the simulation and the results obtained. The analysis was made for a single geometry of after treatment system with three different configuration:

- The first is the baseline configuration, where the exhaust gases leave the SCR outlet and go towards the outlet pipe (tailpipe) without encounter significative obstacles;
- The second is the cone configuration, where the exhaust gases leave the SCR outlet and pass through a restricted section before reaching the sensor location and then the tailpipe;
- The third is the baffle configuration, where the exhaust gases leave the SCR outlet and a plate, placed before the sensor and the tailpipe, obstructs the direct passage of the gases from SCR towards sensor. The gases are obligated to overtake the plate before reaching the sensor location.

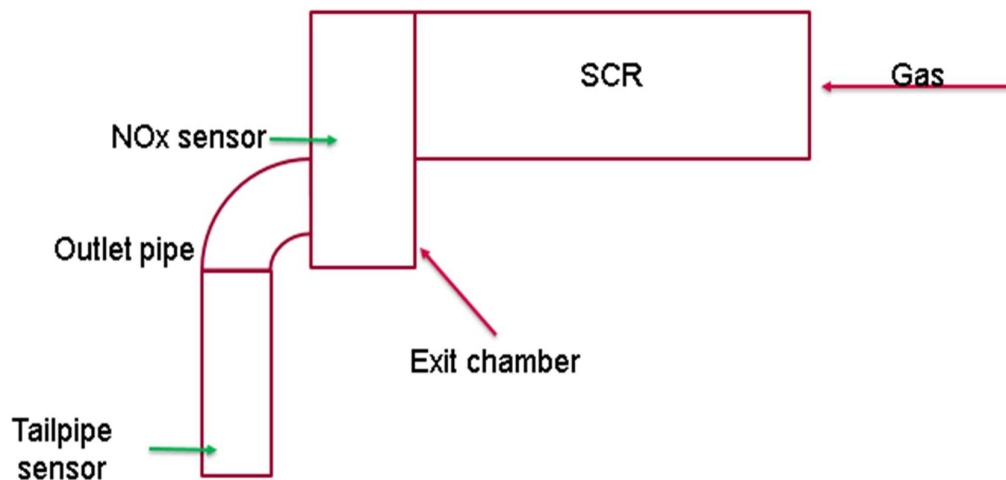


Figure 8.3 Baseline configuration scheme

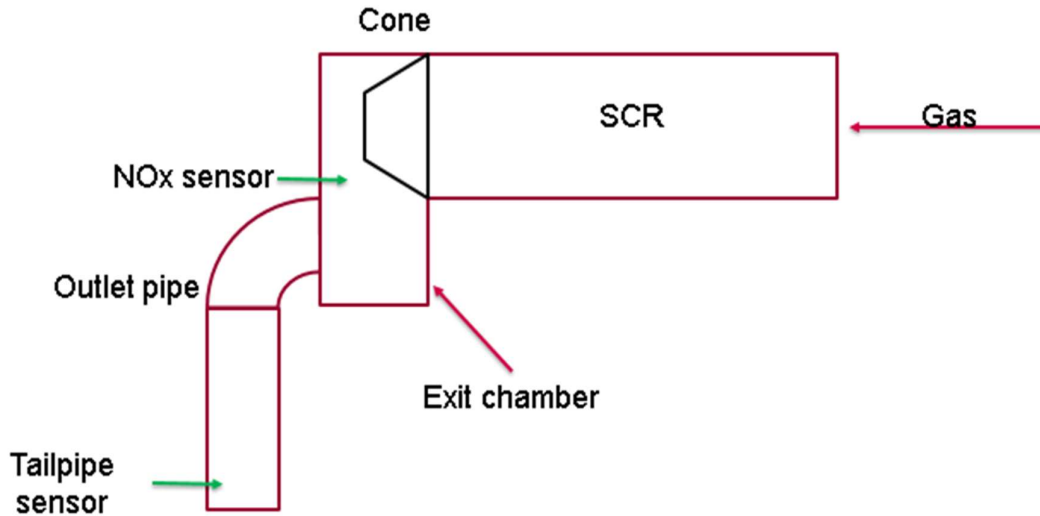


Figure 8.4 Cone configuration scheme

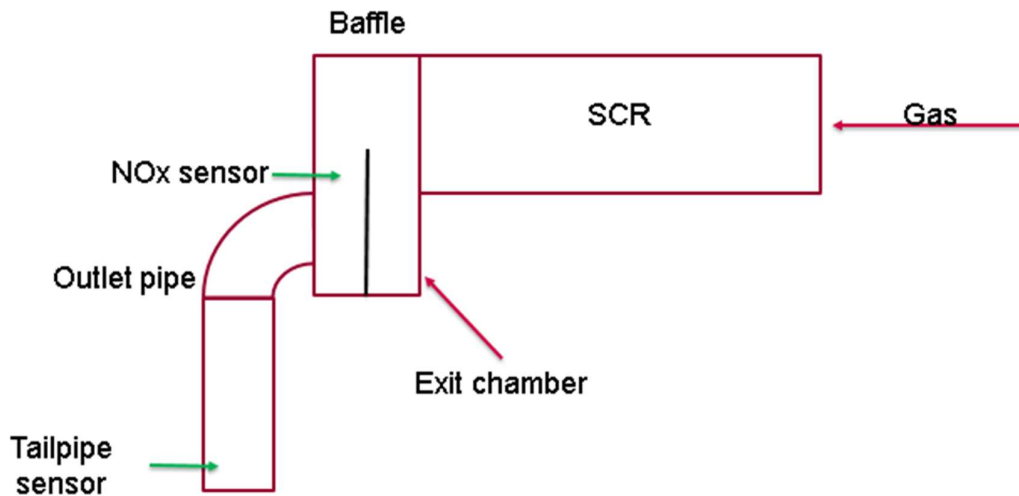


Figure 8.5 Baffle configuration scheme

The aim was to understand which configuration is better for mixing the gases in the sensor location. Test analysis was made and the CFD results will be compared with the experimental data. Test was made considering three velocity operating points. For each point, four different temperatures and torques were imposed. The following plots show the measure done. The value are normalized with a reference value for privacy.

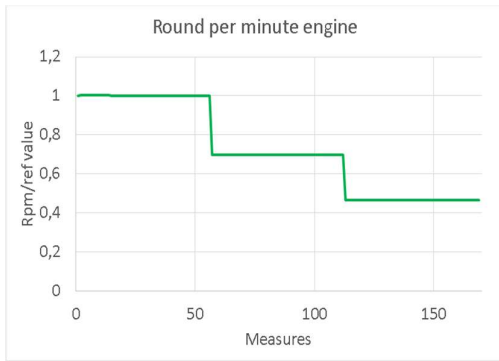


Figure 8.6 Velocity plot

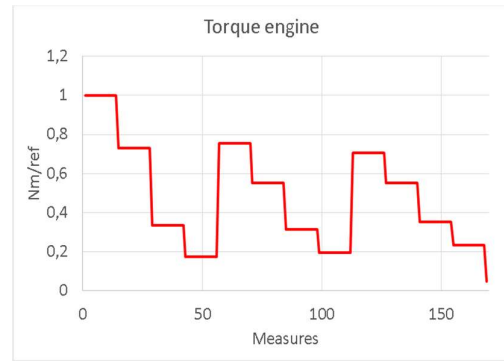


Figure 8.7 Torque plot

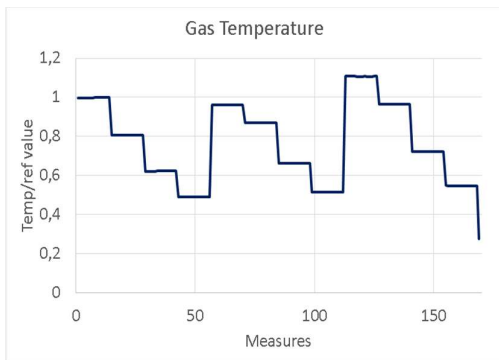


Figure 8.8 Temperature plot

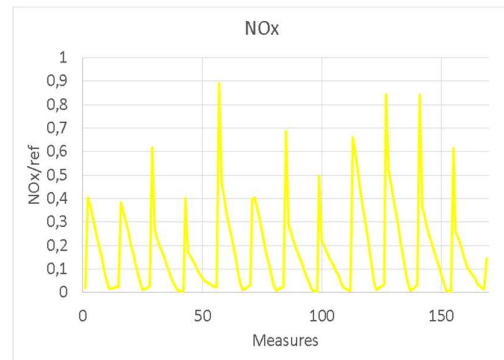


Figure 8.9 NOx plot

The following plot show the measure done by NOx sensor for the baseline configuration. The values measured should respect some limits indicated by the two red line. If the measure is outside these lines, the value measured is wrong.

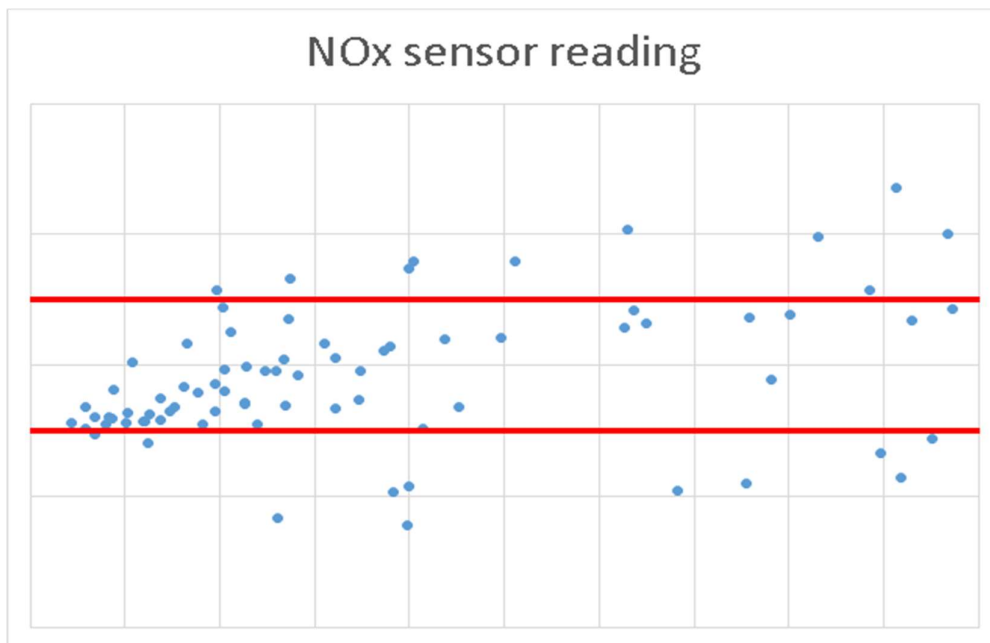


Figure 8.10 NOx sensor reading. Measure and limit to respect

The configurations were tested on bench. The measurements were made relating the values of the NOx sensor in its original position and the values of NOx taken in a position rather far from the sensor, where it is supposed the fluid is fully mixed. From the test bench, the error of the sensor reading between the tailpipe position and the sensor is high for the baseline configuration. The second configuration did not give a great improvement, while the experimental data for the third configuration shown a great improvement.

The same results would be obtained from CFD simulation with the aim to find a methodology and validate the tracer method.

As will be seen and as said before, this method is qualitative and has the only purpose to indicate the discrete point to avoid if it is wanted for the sensor to do properly its job, and the NOx is fully mixed downstream and in the sensor location.

Another application was analysed using the same method with the purpose to examine the mixing of the NOx in more than one section. Indeed, the ATS was mounted on bench with more NOx sensors at different distance from the outlet of SCR. The values of the vehicle sensor was compared with the value of the bench sensor in varying position. The test shown divergent value between all the sensors so an investigation was necessary using the passive scalar tracer method.

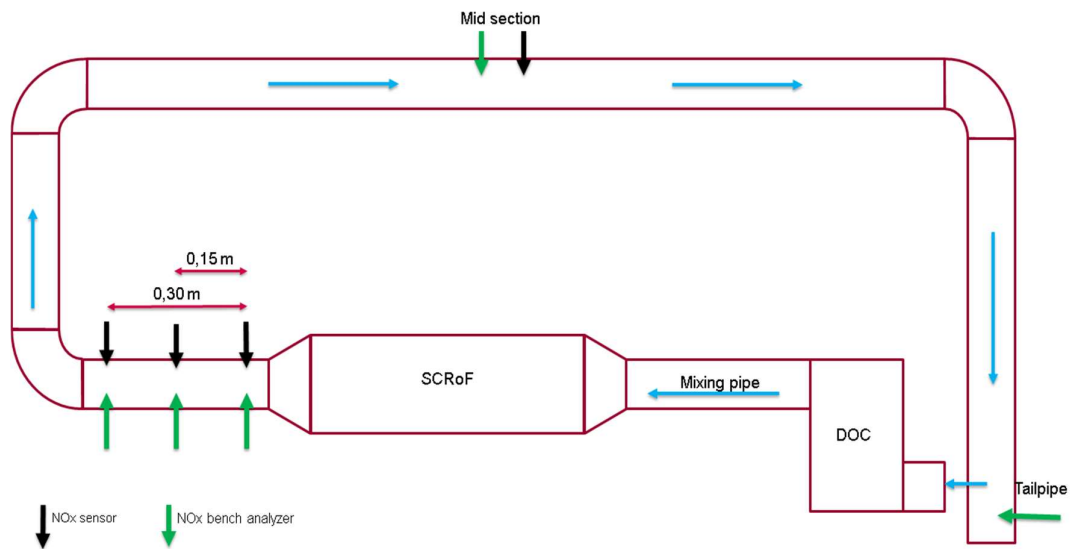


Figure 8.11 Second geometry SCR analysed – scheme.

9. Passive Scalar Tracer Method – First Application

Before starting the simulation, as said in the previous chapters, a pre-processing of geometry preparation is necessary, need to choose the most appropriate discretization of the space and generating a good mesh. An analysis of sensitivity of the mesh should be done, but the computing time will be too much expensive because the case in exam consists of three configurations and three simulations, so three different mesh sensitivities. With reasonable choice, with the experience of the team CFD where this master thesis was developed, and with a good compromise between accuracy and time request for generating the mesh, this one was created using the following models and values:

- Polyhedral Mesher → Mesh size = 3 mm
- Prism Layer Mesher → Layer thickness = 1 mm; Number of layer = 2
- Surface Remesher
- Extruder

The number of total cell is almost 2 million.

The same mesh was done for the three geometry; also, the physical modelling for the simulation was the same. The boundary conditions imposed are the same but the values cannot be reported for privacy. Anyway, the boundary condition imposed on STAR are:

- Mass Flow Inlet → On SCR section
- Temperature → On SCR section
- Pressure outlet → 0 Pa
- Adiabatic wall

The figure below shows the physical model used:

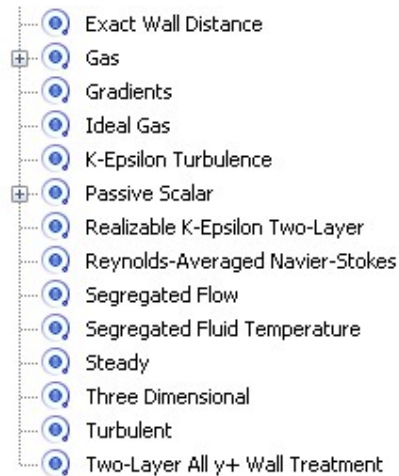


Figure 9.1 Physic models used for the simulation

Each configuration will be described in the following paragraph.

9.1. Baseline Configuration

The first configuration analysed was the baseline, where the fluid flow leave the SCR outlet and through the sensor location going directly on tailpipe. Not the complete ATS was simulated, because this would have required a lot of computational time, so it was supposed a high uniformity at the SCR outlet. Mass flow inlet boundary condition was setted at SCR outlet.

The operating point simulated was the first, where the trade-off measuring was made with high round per minute, high torque and temperature. This is the most problematic point because the sensor here provides bad estimation of NOx.

First step is the sensitivity analysis of the number of passive scalars. The simulation was done subdividing the SCR outlet into 6, 8 and 10 sectors and mean deviation and coefficient of mixing in sensor location was computed. The figure shown the setting of the passive scalar at SCR outlet:

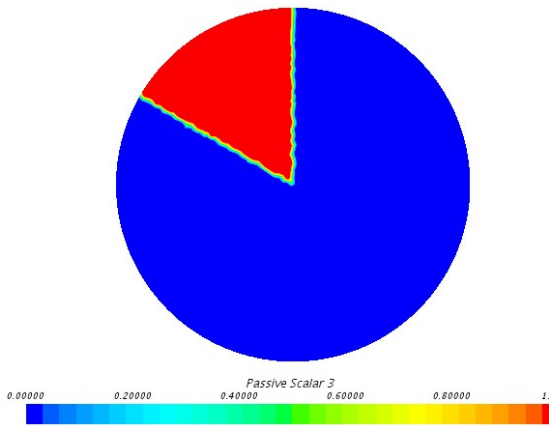


Figure 9.2 Input passive scalar 3

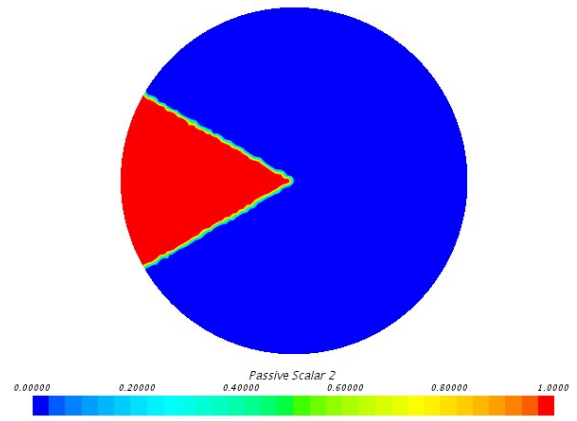


Figure 9.3 Input passive scalar 2

The results are plotted in the following table:

Table 1 Results baseline – sectors

| | CoMix Sensor | CoMix Volume | Uniformity |
|--------------------|--------------|--------------|------------|
| 6 passive scalars | 19.88% | 20.09% | 48.47% |
| 8 passive scalars | 15.49% | 15.88% | 43.34% |
| 10 passive scalars | 21.10% | 22.85% | 45.87% |

The figure below shows the mean deviation of passive scalars on section through sensor.

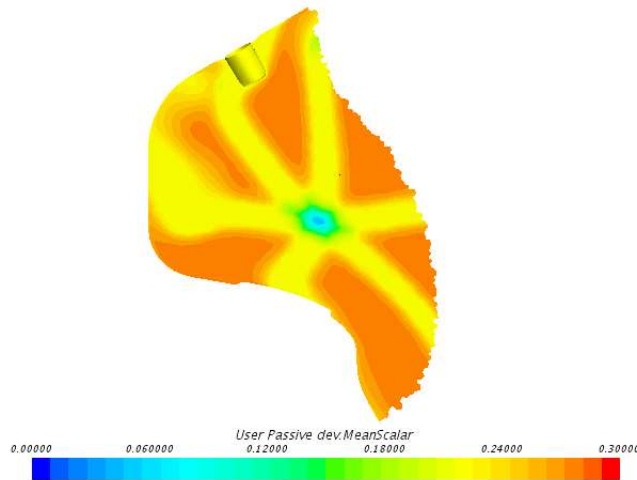


Figure 9.4 Mean deviation section through sensor

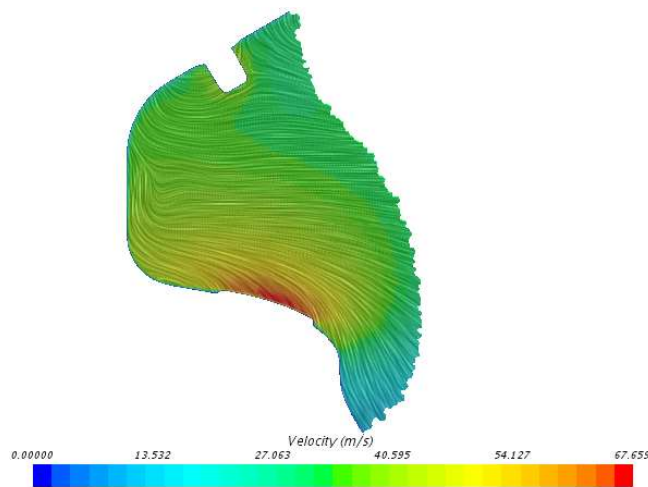


Figure 9.5 Velocity field section through sensor.

The sequent conclusions and observations can be done:

- The first considerations are about the coefficient of mixing. From the results, the coefficient is rather low for this configuration. The target to reach is far from these results, the reading of the sensor could be affected by elevate error.
- Looking the values of mixing on the surface of the sensor, on the volume surrounding the sensor is different. Which value could predict better the real mixing of the gases? Maybe the worst condition must be considered, that is the entire section pass through the section.
- The value of the mixing was computed for the tailpipe section, this section is in a position located far away from the SCR outlet, where it is supposed the fluid fully mixed. As expected, the mixing here is high, almost perfect.
- Looking at the values for different numbers of passive scalars, there are no great variations of the coefficient of mixing. It is possible to verify for this case that there is no sensitivity from numbers of passive scalars.

- The shape of the passive scalars is visible on the figure 9.4. Seems that the fluid does not mix properly before reach sensor location.
- Looking the velocity field, it is linear and maybe this cause the low mixing of the flow (responsible of a good mixing).

Experimental data was qualitatively verified: the sensor in this configuration from CFD does not respect the target imposed.

It is necessary to precise an important observation. The positioning of the sectors was chosen arbitrarily starting from an axis with a specific angle. If another angle or another axis would be chosen, the results obtained would be different! This is an important observation because evidence that this method is totally qualitative (indicate the risk of a bad sensor positioning) and arbitrarily depending on user-defined of how the passive scalars are set.

This observation brings to the second sensitivity analysis based on the shape of passive scalars. The sectors, as said, are very user-depending, need to give some constraints. For example, it could be thought about giving the same aspect of the SCR outlet, or rather circular shape. The only arbitrary choice is, in this way, the number of the passive scalar, which, once defined, provide the radius of every circular shape. The radius is computed in order to obtain the same area like the sectors configuration. The figure of input passive scalars are shows below:

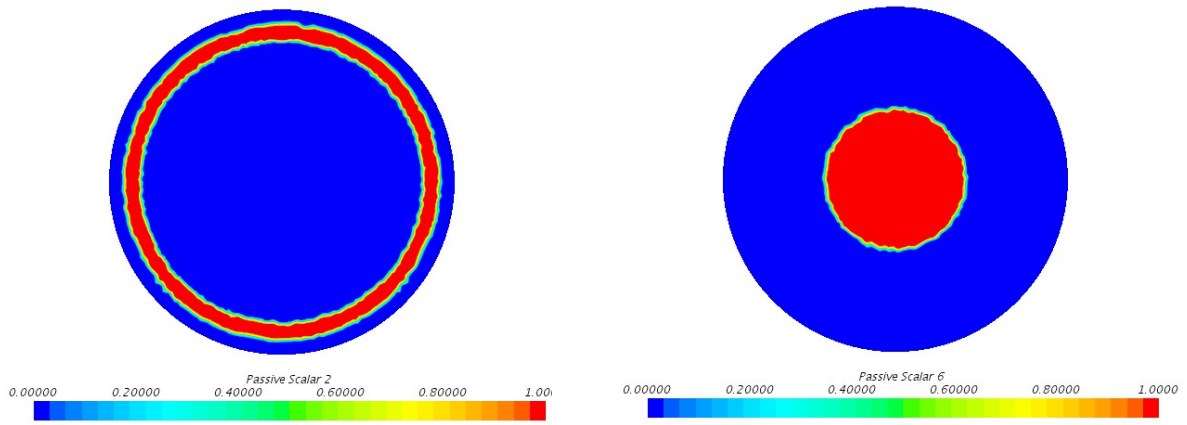


Figure 10 2

Figure 9.7 Input circular scalar 6

The results for this sensitivity analysis are reported on the following table/figure:

Table 2 Results baseline – circular

| | CoMix Sensor | CoMix Volume | Uniformity |
|--------------------|--------------|--------------|------------|
| 6 passive scalars | 26.17% | 27.35% | 76.78% |
| 8 passive scalars | 26.81% | 30.29% | 74.66% |
| 10 passive scalars | 29.3% | 34.43% | 75.22% |

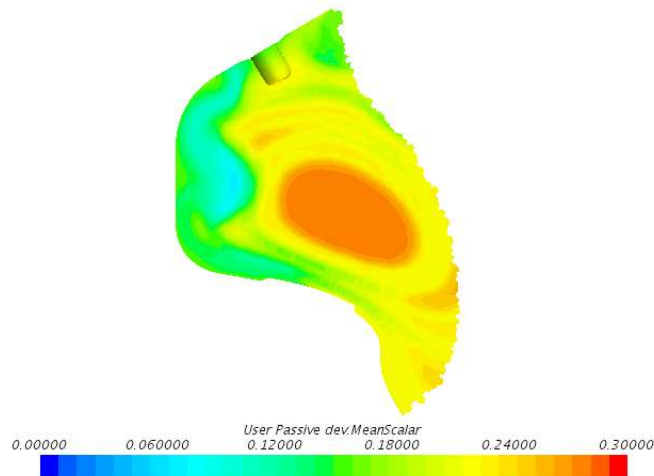


Figure 9.8 Mean deviation section through sensor

The next observations can be done:

- The values of the coefficient mixing is increased compared to of the sector shape configuration. The passive scalar thus distributed seems to mix better. Essentially the passive scalars set up like this, hit much more the zone of the sensor and the mixing results higher.
- As the previous case, the coefficient evaluated on surface sensor, on volume surrounding sensor and on the section passing through the sensor are different but not much each other. The same questions can be done also here.
- On tailpipe section the value of mixing is elevate as in the previous case.
- Also here, changing the number of passive scalars is indifferent, the coefficient of mixing does not vary too much in function of the scalars number.
- The central scalar is visible on section through sensor. Seems that the shape scalars is mixed better than sector scalars.

From this sensitivity analysis, essentially, emerged a raised coefficient of mixing in the sensor location, but not enough to satisfy the target. This is also in line with the experimental data, in which, with this configuration the sensor does not read a good value of NOx.

It can be noticed that, this configuration does not match the real distribution of NOx and could be not the worst scenario to represent (like sectors shape). Indeed, it is only another arbitrary input imposed at SCR outlet section. The real distribution cannot be measured and these are only hypothesis which confirms that this method is only a rapid way to indicate where and where not locate the sensor (as repeated more and more time before).

9.2. Cone Configuration

The second configuration considers a restrict area at the SCR outlet, with the purpose to direct the flux towards the NOx sensor location. The results from test bench were not so much satisfying, the solution adopted did not provide any improvement compared to the baseline configuration. The analysis CFD for this configuration is here reported and analysed. First step the sensitivity from number of scalars for the sector shape:

Tabella 3 Results cone – sectors

| | CoMix Sensor | CoMix Volume | Uniformity |
|--------------------|--------------|--------------|------------|
| 6 passive scalars | 25.76% | 32.95% | 62.59% |
| 8 passive scalars | 28.7% | 31.63% | 59.42% |
| 10 passive scalars | 30.74% | 30.92% | 58.15% |

The figures below shows the mean deviation of the passive scalars on section through sensor:

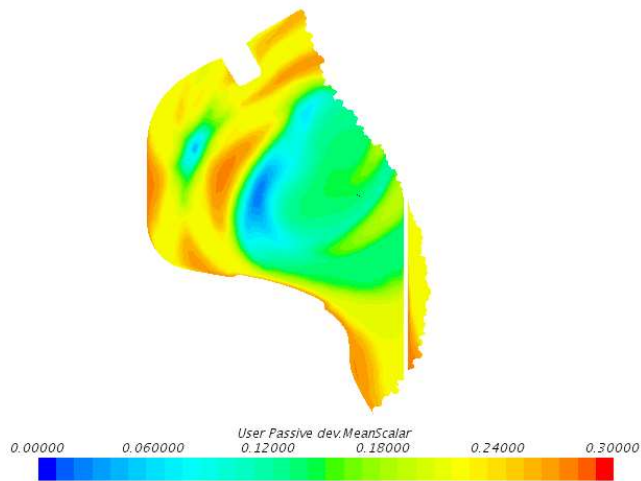


Figure 9.9 Mean deviation section through sensor

And the velocity field:

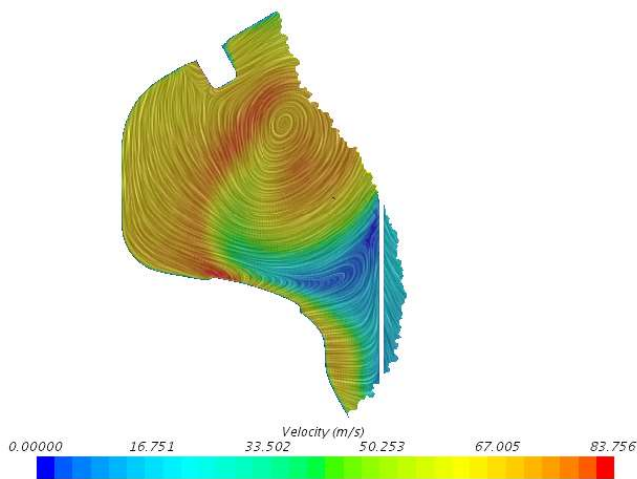


Figure 9.10 Mean deviation section through sensor

The following observation can be done:

- The values of the coefficient of mixing for this configuration is higher than the baseline configuration, but not in target. In this case the CFD analysis provides a result that is not expected because from the experimental data there was no improvement, instead the CFD shown a better coefficient of mixing. It would be useful investigate on this results and on experimental data. Anyway, the method used as indicator of risk is working.
 - Looking the values of coefficient of mixing on sensor surface, on volume surrounding the sensor, they are rather different compared to the baseline configuration. The surface coefficient of mixing is the highest, the volume instead loses ten percentage points.
 - The values of the coefficient of mixing here are also elevate on tailpipe zone.
 - The number of passive scalars here is also indifferent, the values change of some percentage point.
 - The velocity field is higher, and more direct on sensor, but not a good mixing is reaching
- The successive step is to change the shape of the passive scalar and impose a circular area. The results are plotted below:

Table 4 Results cone – circular

| | CoMix Sensor | CoMix Volume | Uniformity |
|--------------------|--------------|--------------|------------|
| 6 passive scalars | 53.04% | 41.43% | 62.22% |
| 8 passive scalars | 49.7% | 41.05% | 62.68% |
| 10 passive scalars | 52.7% | 47.17% | 61.6% |

The mean deviation is reported below:

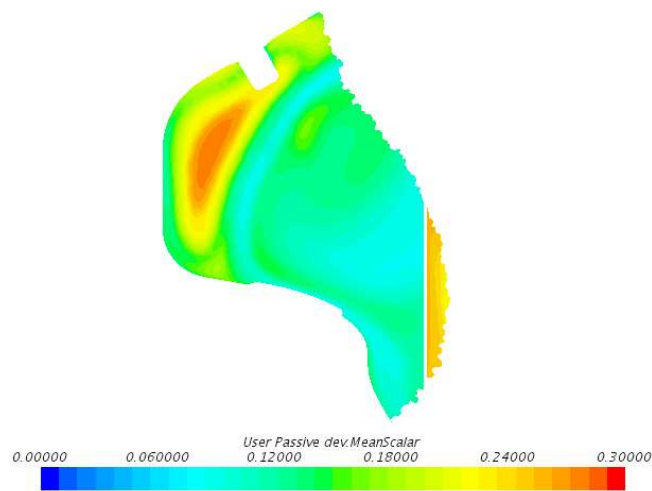


Figure 9.11 Mean deviation section through sensor

The following observation can be done:

- The values of the coefficient of mixing improved, it almost redoubles the values of sector shape. Results are not in target but the CFD data shown an improvement of the mixing for this configuration. Again, the indicator of risk is working, and the NOx measures of this configuration could be wrong.

- Looking at the values of coefficient of mixing in different positions, they have the same trend of the previous analysis. The surface sensor provides the best coefficient of mixing, whereas the volume provide lower value.
- Same consideration can be done for tailpipe section. High value of mixing here.
- Number of passive scalars did not influence too much the simulation. The results do not change considerably.
- The section seems to be more mixed with this scalar. The high value of the mean deviation is moved toward the sensor.

9.3. Baffle Configuration

The third and last configuration considers a plate between the SCR outlet and the zone of the NOx sensor. The most of fluid in this case must overtake the plate before reaching the sensor location and go out through tailpipe. From test bench this configuration provided great improvement. The same results are expected from CFD simulation, with the purpose to satisfy the target condition.

Also for this configuration, sensitivity analysis was done both for number of passive scalars and shape of the passive scalar input to set up on SCR outlet.

The results are plotted here:

Tabella 5 Results baffle – sectors

| | CoMix Sensor | CoMix Volume | Uniformity |
|--------------------|--------------|--------------|------------|
| 6 passive scalars | 52.68% | 59.58% | 89.45% |
| 8 passive scalars | 52.9% | 61.28% | 89.84% |
| 10 passive scalars | 53.04% | 59.62% | 88.73% |

The mean deviation is reported below:

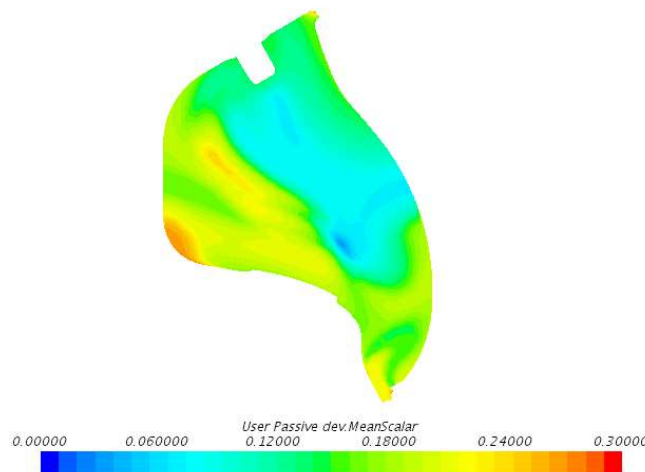


Figure 9.12 Mean deviation section through sensor

And the velocity field:

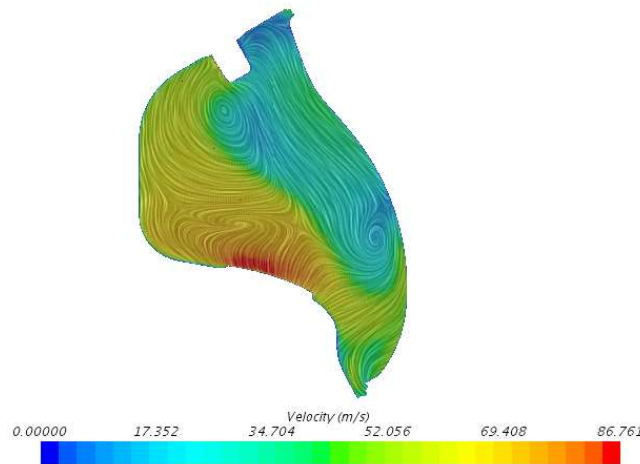


Figure 11

The following observation can be done:

- The coefficient of mixing is the highest compared to the other configurations, but the value, also here, does not respect the target to reach, so the NOx sensor will have problem on reading.
- Looking at the values of mixing on the surface of the sensor, on the volume surrounding the sensor and on the section through the sensor, they are different. They are increased in comparison to the other configurations.
- The value of the mixing for the tailpipe section is in line with the other configurations and it is elevate. This indicates that in tailpipe zone the fluid is fully mixed.
- Looking for the values for different numbers of passive scalars, there are no great variations of the coefficient of mixing. There is no sensitivity from numbers of passive scalars.
- The velocity field seems to be more turbulent and the mixing is high. The mean deviation is low on sensor location, but looking the section through sensor it is not uniform.

The next step is to change the shape of passive scalars input, imposing a circular shape passive scalar. The results are shown in the following table:

Table 6 Results baffle – circular

| | CoMix Sensor | CoMix Volume | Uniformity |
|--------------------|--------------|--------------|------------|
| 6 passive scalars | 76.03% | 78.35% | 90.56% |
| 8 passive scalars | 73.1% | 74.82% | 90.54% |
| 10 passive scalars | 78.9% | 78.08% | 88.74% |

The mean deviation is shown below:

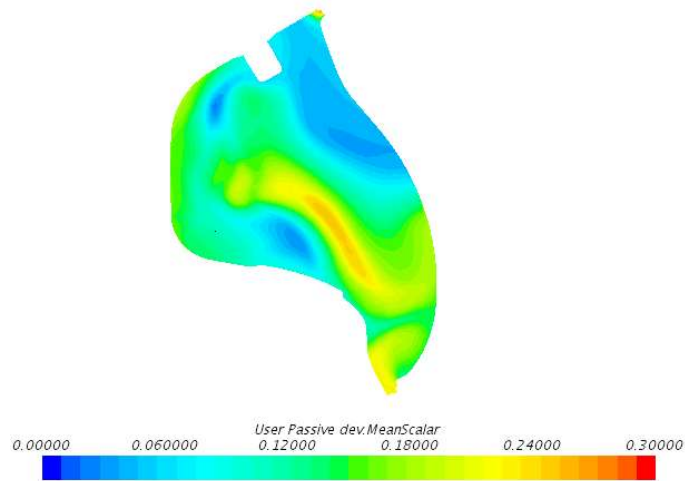


Figure 9.14 Mean deviation section through sensor

The following observations can be done:

- The coefficient of mixing, like in the other configuration, increased until reaching the target value. In this simulation, with this set up of passive scalars, the baffle configuration results the only one that respects the target and the NOx sensor will read correctly the NOx concentration.
- The value of mixing computed on the different zones confirms the trend of the previous simulation. The value increases (only a few percentage point) for the volume surrounding the sensor.
- The mixing at tailpipe is quite high like in the other configuration and simulation.
- Number of passive scalars does not influences the results, they change only for a few of percentage points. In addition, for this simulation there is not a great sensitivity due to number of passive scalars.
- The mean deviation here seems more uniform then previous analysis, so this can explain the high mixing coefficient values.

9.4. General Conclusions

In conclusion, the results obtained and shown in the previous paragraphs are below summarized.

As explained, the problem born when NOx concentration measured by vehicle sensor, was different by NOx concentration measured on tailpipe section. Various geometric configurations are adopted in order to solve the problem. The first configuration considers a cone which, placed directly on SCR outlet, restricts the exhaust gases and directs them on sensor location. The results were poor, this configuration does not bring any significant improvement. The second configuration adopted considers a plate, which located between SCR outlet and sensor position, imposed the most part of exhaust gases to overtake this plate before reaching the sensor location and then pass through outlet pipe. The results were good, the error between vehicle sensor and tailpipe was reduced and the target of accuracy reached.

The purpose of this CFD analysis was to understand why NOx sensor on baseline and cone configuration provides wrong measure, instead in the baffle configuration the NOx sensor

reading was in line with the tailpipe section values. The analysis done, has had as purpose to find also a methodology to avoid problems of NO_x sensor reading and define a good indicator that can properly describe the mixing of gases on sensor location.

The simulations, as seen, are independent by number of scalars used. Increase the number of sectors means simply that the NO_x, by the hypothesis done, are concentrated on a smaller area of the SCR surface outlet. Consequently, the uniformity of NO_x distribution on SCR outlet is lower and, independently of the passive scalars number, the coefficient of mixing computed is almost the same on different sections.

Quite the opposite are the results changing the shape of passive scalars input. All the simulations showed an increase of the coefficient of mixing, and only with this setting the baffle configuration reach the target of mixing on sensor location.

The reason why circular scalar better mix and reach the sensor location could be the greater boundary between the zone with NO_x and the zone without NO_x, and simply the diffusion is greater for this matter.

Looking instead at the trend of values, the experimental results are validated. The coefficient of mixing is quite high for baffle configuration; cone mixing is greater than baseline even if the experimental data shows no difference between the two configurations . This method is strongly dependent on the NO_x distribution on SCR outlet, so further studies are necessary.

The conclusion of this analysis is that the method is a discrete indicator of fluid mixing, on tailpipe section, the mixing is high (as expected from experimental data), and on sensor location can give an index of good/bad mixing.

In the next chapter the same method was applied on another geometry, successively the urea injection was simulated with simple hypothesis. The purpose was to find a real NO_x distribution at SCR outlet, based on NH₃ distribution at SCR inlet.

10. Passive Scalar Tracer method - Second Application

Passive scalar tracer method explained in the previous chapter, is here used for another application. The ATS tested on bench has more NO_x sensors (vehicle and bench) in more sections, with the purpose to measure the NO_x concentration not only in the original sensor location but also in other location and evaluate the mixing of the fluid. Simulated geometry had two SCR in parallel placed with a certain outlet distance.

More turbulence models were used with the aim to evaluate the impact on coefficient of mixing. The figure shows the geometry analysed.

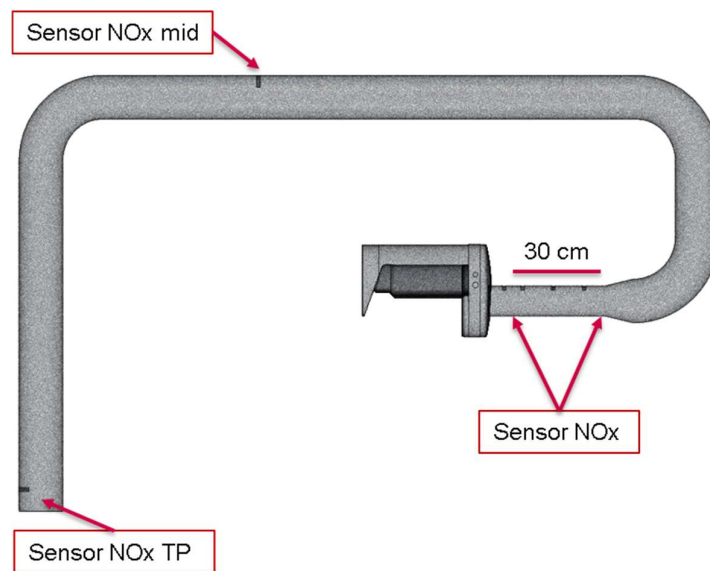


Figure 10.1 Geometry after SCR with sensor location

The mesh size is 4 mm with polyhedral generator mesh and prism layer mesh composed by 4 layer with the first layer thickness of 0.2 mm. Boundary condition again cannot be shows, but the mass flow inlet here was splitted on two SCR section.

Coefficient of mixing and velocity field were analysed on different sections in order to find a relation with experimental data.

Passive scalars were imposed on SCR outlet subdividing each section in four sectors (with in total eight scalars). For each sector, the scalar value of one was imposed and coefficient of mixing was evaluated only on the section of interest.

The experimental data shows reading error on different sections, the error can be reported on following graphic:

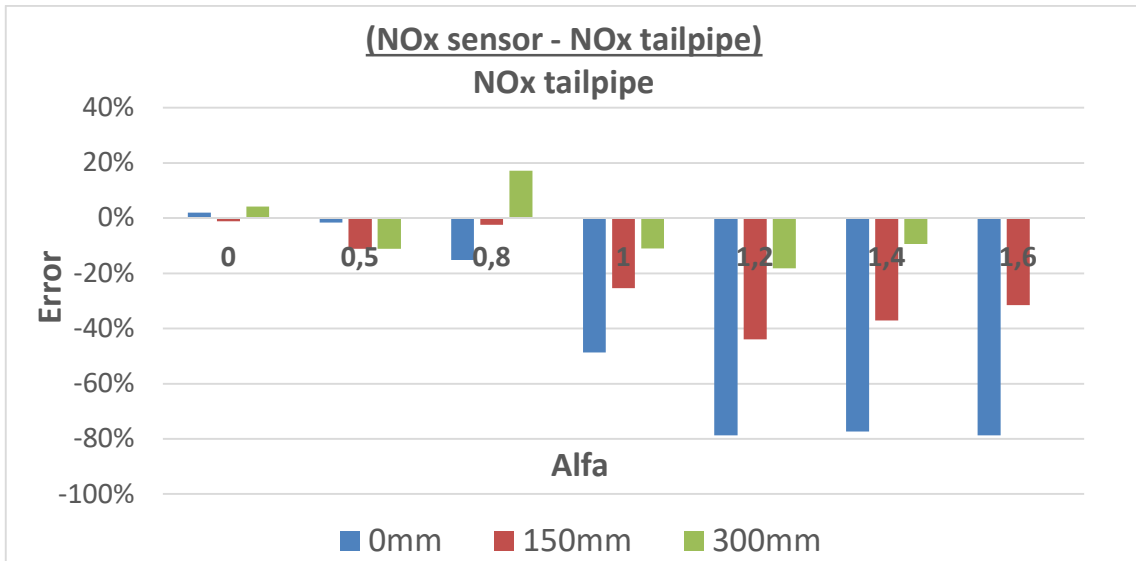


Figure 10.2 Error sensor reading on different position. The error was computed in relation of the value at tailpipe section

Where different measure was done changing the α urea injected. The error is low at low α , but increase a lot with high value of α . The error is reduced along the outlet pipe; mid sensor and tailpipe sensor measure provided the same values. The purpose of tracer method is to find a trend of coefficient of mixing that reflects the testing data. The results will be described in the following paragraph.

10.1. *K-ε Model Analysis*

As explained in previous chapter, k-epsilon model is the most used turbulence model. It describes turbulence using two equation, one for kinetic turbulence and one for dissipation rate of turbulence.

The table below shows the results obtained of coefficient of mixing. In the same table are reported the uniformity index of the velocity on different section.

Tabella 7 Results mixing and velocity on different sections

| | Sensor 1 | Sensor 15 cm | Sensor 30 m | Sensor TP |
|-------------|----------|--------------|-------------|-----------|
| CoMix | 33.24% | 50.1% | 57.7% | 99.6% |
| UI Velocity | 76.7% | 87.5% | 90.9% | 96.2% |

The figure below shows the scalar input on two SCR. Total scalars are 8:

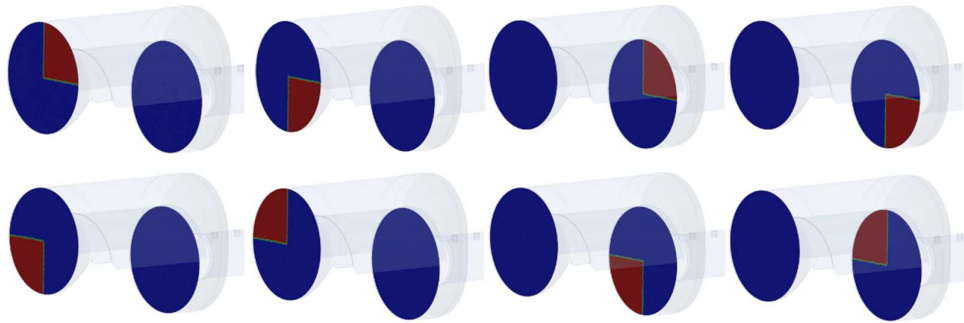


Figure 10.3 Input passive scalars SCR

The figure below shows the velocity field and the mean deviation for every section.

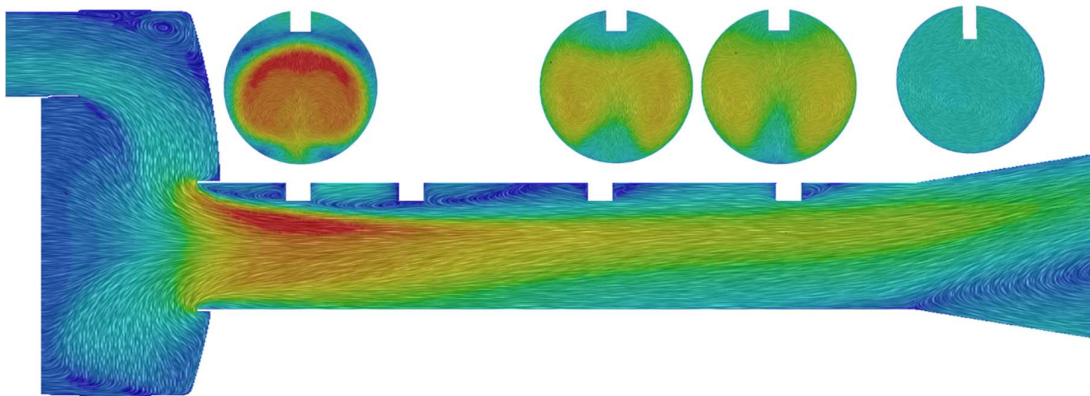


Figure 10.4 Velocity profile. From left: Sensor 1; Sensor 0.15 m; Sensor 0.3 m; Sensor TP

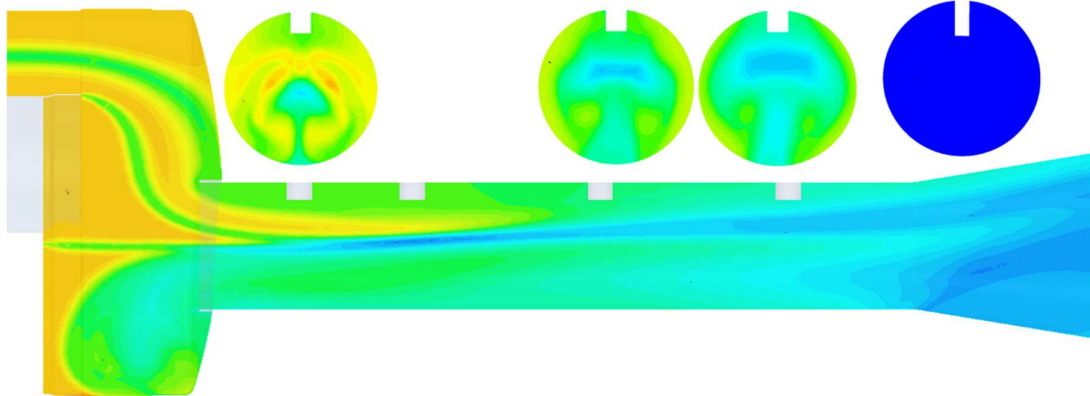


Figure 10.5 Mean deviation. From left: Sensor 1; Sensor 0.15 m; Sensor 0.3 m; Sensor TP

From SCR outlet, the gases are constraint to pass through a restricted section before reaching the sensor location. This cause separation of fluid flow and the stream is mainly concentrated in the center of pipe (look the first section). The sensor located here is the one most affected by reading error. Looking the other sections, the velocity field become more uniform. The fluid

pass through sensor location and the measures are less affected by reading error. Also, the mean velocity is lower. Looking at the mid and tailpipe section, the velocity is perfectly uniform with halve mean velocity.

Similar observations can be done for coefficient of mixing. The mixing is low on first section, the mean deviation of the scalars is high almost in the whole section, the uniformity is low and consequently the mixing is low.

Along the pipe, the mean deviation decrease, the uniformity increase and the coefficient of mixing grown to 50% on section at 0.15 m from SCR outlet, and to 57% on section at 0.3 m from SCR outlet.

Tailpipe section and mid section provide high values of mixing, as expected from test data. The tracer method, also here, is a valid indicator of the risk of sensor positioning. The only problem is that it is a qualitative method; the error of sensor reading does not correlate with the grade of mixing.

10.2. $K - \omega$ Model analysis

In order to evaluate the sensitivity of coefficient of mixing respect the turbulence model. The results are shown on table below:

Tabella 8 Results mixing and velocity on different sections

| | Sensor 1 | Sensor 15 cm | Sensor 30 m | Sensor TP |
|-------------|----------|--------------|-------------|-----------|
| CoMix | 33.24% | 50.1% | 57.7% | 99.6% |
| UI Velocity | 76.7% | 87.5% | 90.9% | 96.2% |

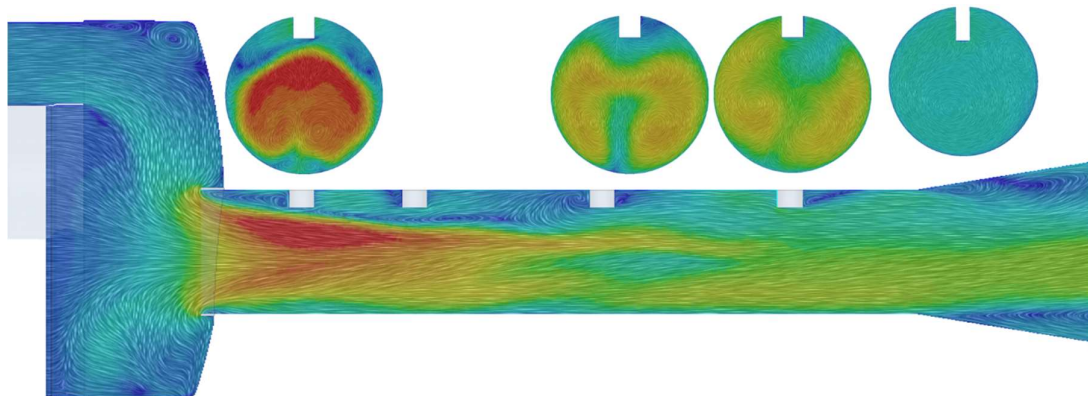


Figure 10.6 Velocity profile. From left: Sensor 1; Sensor 0.15 m; Sensor 0.3 m; Sensor TP

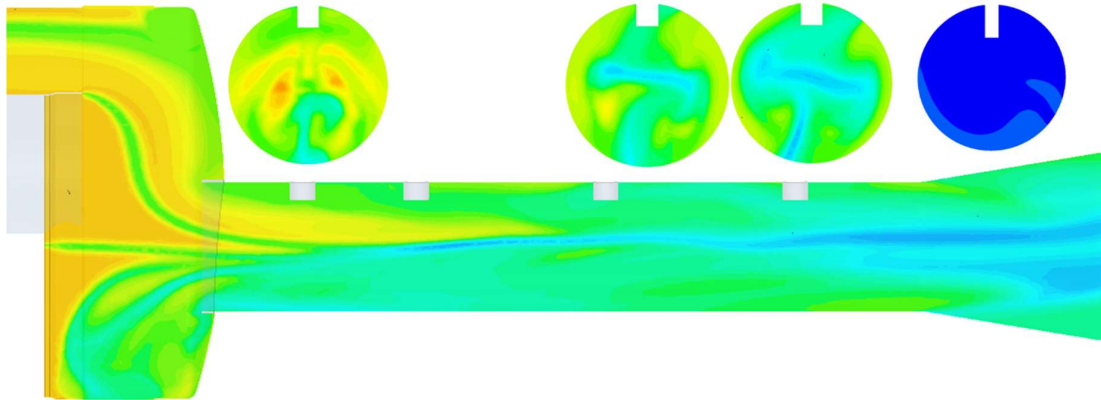


Figure 10.7 Mean deviation. From left: Sensor 1; Sensor 0.15 m; Sensor 0.3 m; Sensor TP

The velocity profile is similar between the two models, the $k - \omega$ is able to compute some eddies respect $k - \epsilon$. The maximum mean value of velocity is the same; it is possible to see the separation of the fluid flow at the inlet of the pipe. Like the $k - \epsilon$, the velocity is greater in the centre of the pipe, so this mean that the NOx concentration is located in this zone.

Coefficient of mixing is quite the same; the difference between the two models is a matter of a few percentage points. There is no sensitivity about the turbulence models chosen.

Mid and tailpipe section mixing is high as expected and like the $k - \epsilon$ model.

The same observation done for $k - \epsilon$ turbulence model analysis can be done for $k - \omega$.

The simulations done demonstrated the test data, which evidenced the error reading of NOx sensor compared to the value measured on mid of the outlet pipe. The mixing is low, confirming the test data. An interesting observation can be done if the isosurface of the passive scalar with target value is plotted.

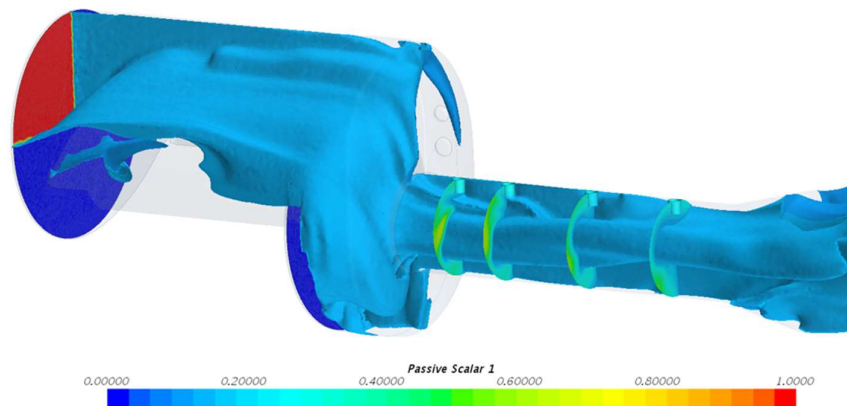


Figure 10.8 Isosurface passive scalar from SCR 1 with value = 0.125

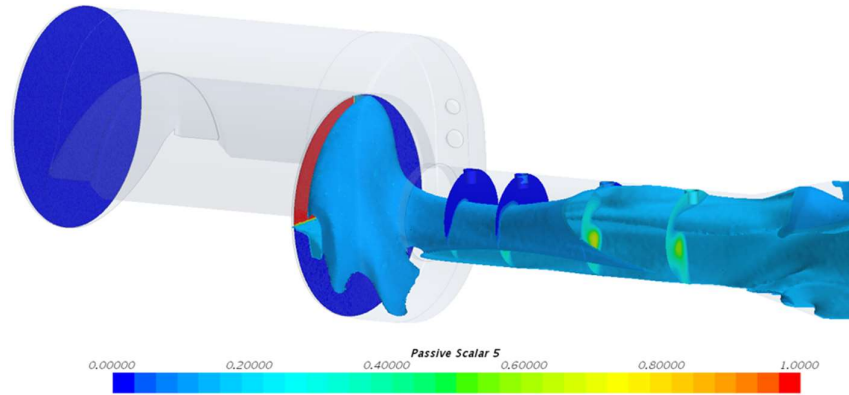


Figure 10.9 Isosurface passive scalar from SCR 2 with value = 0.125

In the scene two passive scalar, one exiting from the first SCR outlet, one exiting from the second SCR outlet, are showed. The value of the isosurface is equal to the target value that hypothetically the sensor should be reading if the mixing was high. Passive scalar come from the distant SCR outlet, has the time to develop on the casing and it reaches the sensor location. Passive scalars come from the near SCR outlet, has no time to develop and the target value does not hit the sensor positioned on pipe.

The bad grade of mixing could be the excessive restriction of the pipe, or in this case, the NO_x from near SCR outlet do not have time to mix, but the real distribution is unknown so this analysis remain qualitative.

For a more realistic simulation of the mixing of NO_x, would be useful to find the distribution of NH₃ at SCR inlet, then with simply hypothesis, obtain the distribution of NO_x at SCR outlet.

11.NH3 Injection Simulation

The purpose of simulate the NH₃ injection is to understand the uniformity index of the NH₃ at SCR inlet, and with simple hypothesis, find the “real” distribution of NO_x at SCR outlet. The reason is that a high uniformity means that the gases are better mixed and conversion of NO_x inside SCR is higher.

The simulation of injection is not simple, and a complete simulation, would need more models for the evaluation of liquid film, solid region for evaluate the heat transfer caused by the liquid injected (with low temperature compared to the operating temperature of gas). The more complicated is the simulation, the more is the time needed to compute the solution.

Urea injector usually works with logic ON/OFF based on the alpha desired for the abatement of NO_x. Dosing module provides a constant mass flow rate, using this logic it is possible to choose the duty cycle for the desired mass flow rate and the injection law becomes a square wave signal. For simplicity, it was computed the mass flow rate injected without considering this law and imposed constant mass flow rate from the injector.

The mesh created is a 4 mm cell size, with four layers and size of the first layer equal to 0.2 mm. The injection simulated is simple; the Bai-Gosman model was used with evaporation model and TAB break up model for the droplets break up. No liquid film was analysed, the mixer inside the fluid region was modelled with solid region and the temperature monitored. Interface and wall boundary condition for the Lagrangian particles was setted up with Escape condition. This condition eliminates the particles that hit the wall; the incident mass flux was monitored and then imposed like flux of species. Still for simplicity, the liquid injected is H₂O and the process of urea thermolysis and hydrolysis was not considered.

The simulation was run in steady state, and in transient state. The number of parcels was set up on 60 parcels. The particle size was set up using cumulative function distribution (CFD) gets from producer of dosing module. The particles temperature was set equal 60 °C. For transient state time step used was 0.001 s and stop time criteria of 2.5 s.

The following paragraphs will analyse the results obtained.

11.1. Steady State Injection

The purpose is to evaluate the distribution of H₂O on SCR inlet section. The mass fraction and the mean mass fraction was monitored to evaluate the convergence of the simulation. The steady simulation required a lot of computational time even for a simply injection like this. The time used was more than 60 hours using 64 core processor. The mass fraction graphic it shows below:

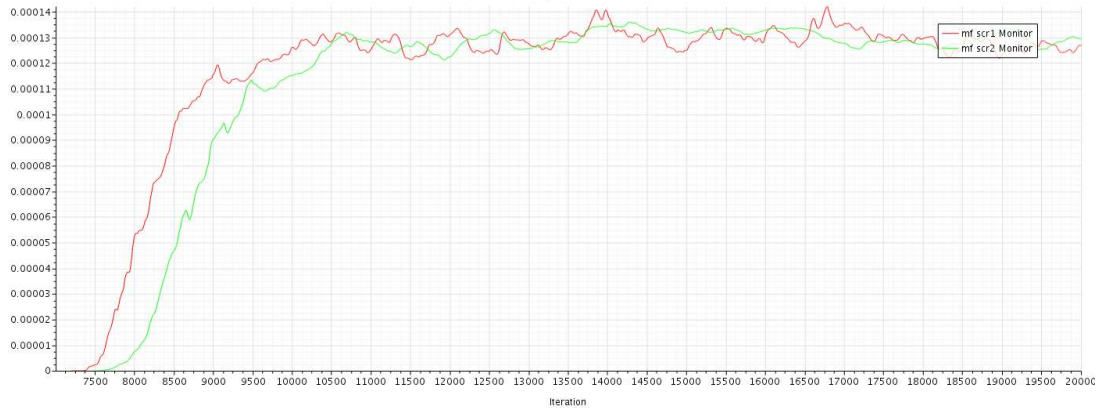


Figure 11.1 Mass fraction H2O computed on SCR section. Red SCR1, green SCR2.

The convergence is reached after 4000 iteration, but the values of instantaneous mass fraction are quite fluctuant. The second SCR mass fraction value fluctuate with a low frequency. The results are fluctuant probably because the velocity field before reaching the SCR inlet is too much variable with a lot of eddies and the software is not able to find a unique solution. Looking at the distribution, it changes at every iteration, even if it fluctuate around a mean value; this means that convergence has been reached.

Looking at uniformity, it is high for both SCR inlet, but the distribution of the second seems to be more uniform without great difference between max and min value of H2O mass fraction.

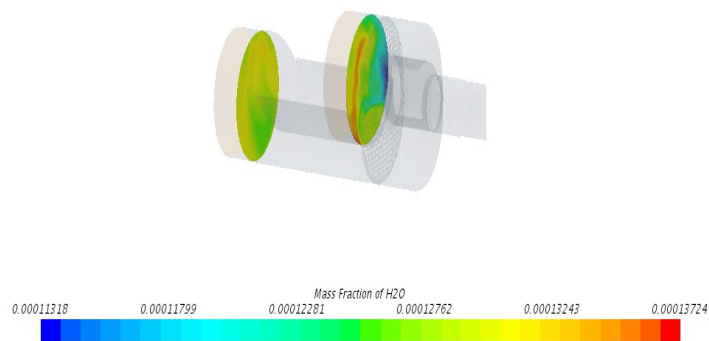


Figure 11.2 Distribution of mass fraction of H2O on SCR inlet

This distribution will be imposed on SCR outlet with the assumption that not all the NOx will be reduced. The chemistry and the balance of the reduction equation will be neglected; only simple hypothesis will be done.

11.2. Unsteady State Injection

The same simulation but with unsteady state solver was started. The purpose, also here, was to evaluate the distribution of H₂O on SCR inlet. The results are here showed and analysed

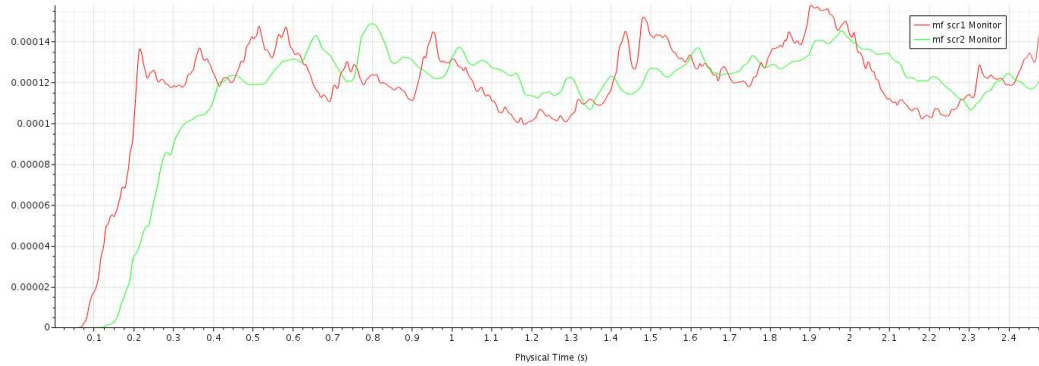


Figure 11.3 Mass fraction unsteady state.

The mass fraction, compared to the steady state simulation, fluctuate more in function of time. The mass fraction on SCR 2 is less unstable, the response of the system is unstable and the solution does not reach a unique value.

Looking instead at the value of mass fraction, the mean value on section is similar between the steady and unsteady simulation.

Different photo of the distribution was saved during the simulation. The distribution of H₂O is variable and never reach a unique solution. Even if the mass fraction change during the iteration, essentially on SCR 1 has great value and low value of mass fraction on ALTRE IMMAGINE, as it is possible to see on figure below:

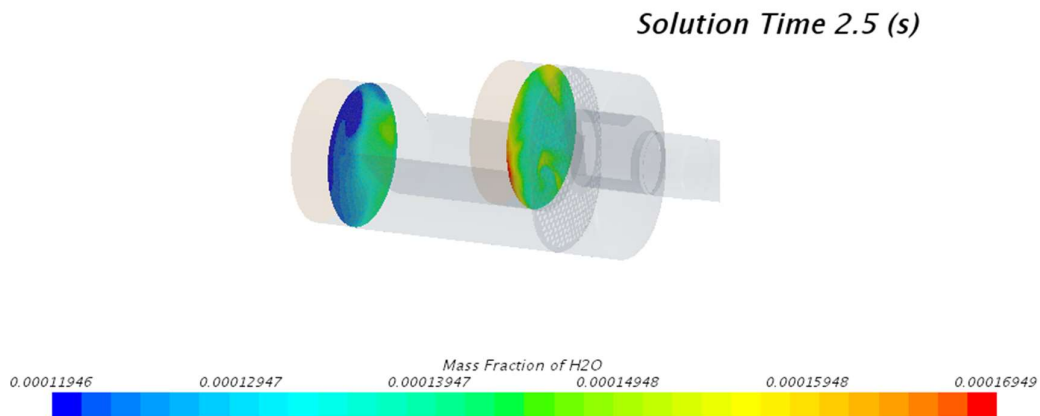


Figure 11.4 Mass fraction SCR unsteady. Solution time 2.5 s

The distribution on SCR 2 instead seems to be more uniform in comparison with the SCR 1. The fluid flow like the analysis done for the tracer method, has time to develop inside the SCR casing, reaching the SCR section uniformly.

Last chapter will describe the last simulation done, where the NO_x distribution was imposed at SCR outlet.

12.NOx Distribution at SCR outlet – Mixing

From the previous chapter, a simplified injection was simulated and distribution of NH₃ (H₂O simulated instead of NH₃ for simplicity) was computed. The NH₃, as seen, reach a high uniformity, this means that the NO_x conversion inside the SCR will be quite high.

To find a real distribution of NO_x is very difficult, for the simple reason that a good chemistry model would be needed. Simulate and resolve all the main reductive equations is very complicated and surely, the time for the computing will be very expensive. Instead, the simulation done for this master thesis treated only the flow of exhaust gases.

The value of H₂O mass fraction was extracted from SCR inlet, the average value computed. From average value, it was taken a range of +/- 3% of mass fraction, the logic is that if the mass fraction is too low, the NO_x are not reduced and if the mass fraction is too high, the NO_x are not reduced.

The distribution derived was imposed as passive scalar at SCR outlet and another simulation was set up. The solution are here plotted:

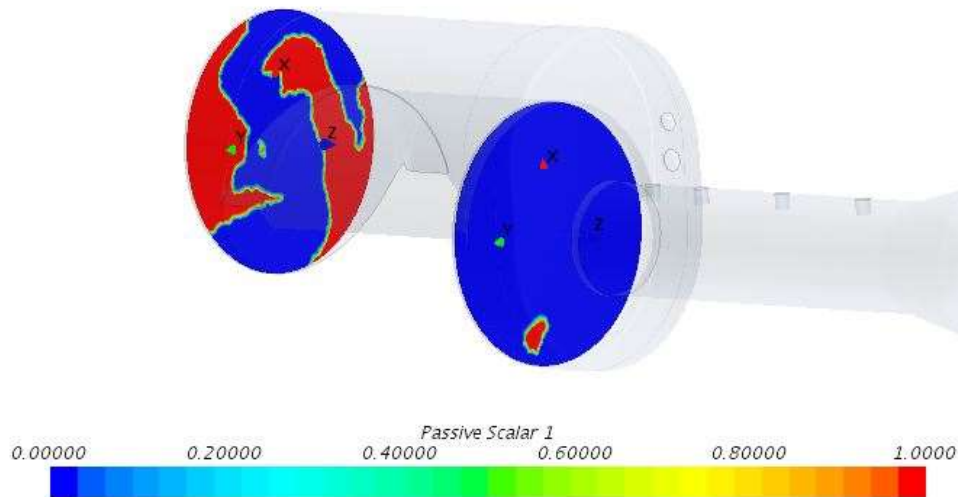


Figure 12.1 NO_x distribution SCR outlet

The first figure shows the distribution that was obtained and imposed to SCR outlet section. The SCR 1 from previous analysis resulted less uniform respect SCR 2, so NO_x mainly come from SCR 1. As seen from the first passive scalars method, it is expected that the distribution has time to develop before reaching the striction of the outlet pipe.

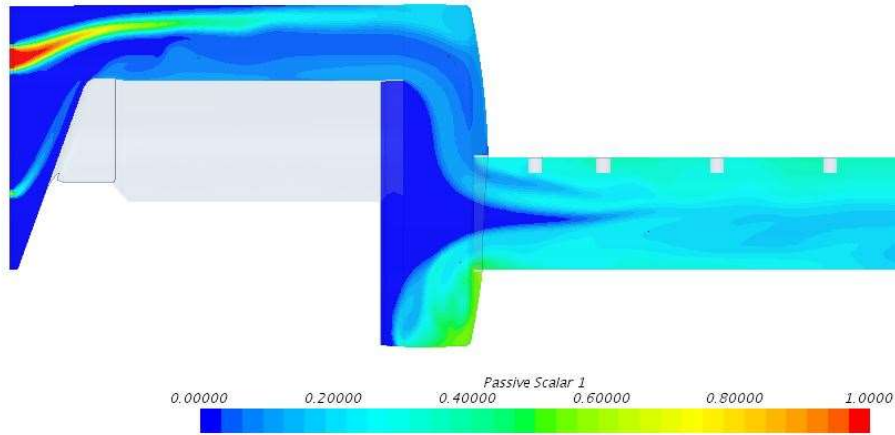


Figure 12.2 Passive scalar distribution inside the pipe

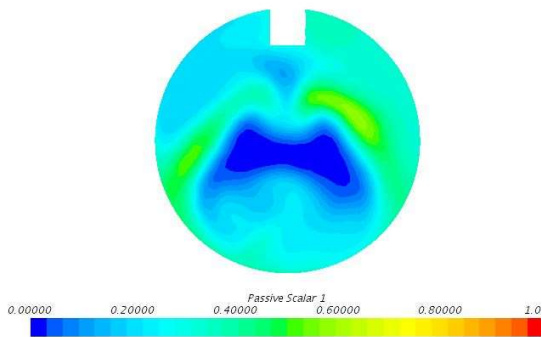


Figure 12.3 Section sensor 1

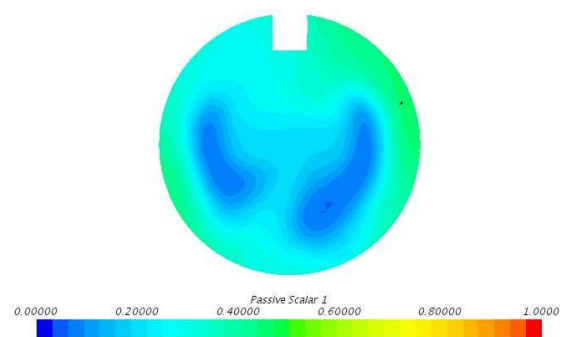


Figure 12.4 Section sensor 0.15 m

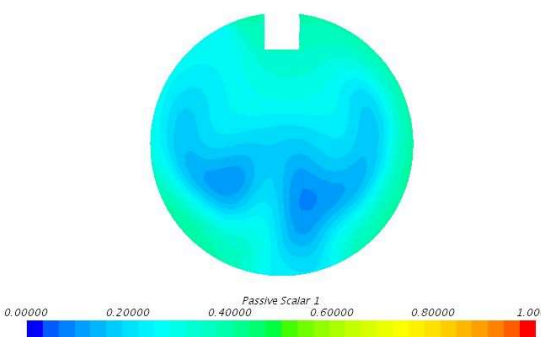


Figure 12.5 Section sensor 0.3 m

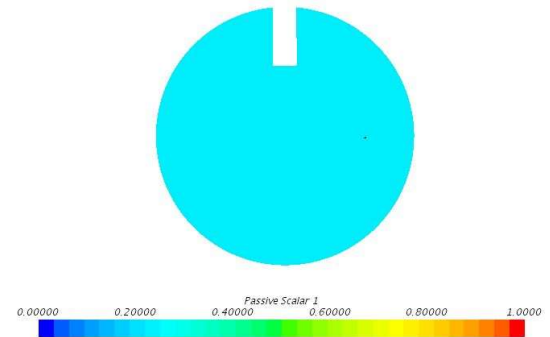


Figure 12.6 Section sensor TP

Looking at the sensor section, the passive scalar value is near to zero in the centre of the pipe. The successive sections showed instead how the passive scalar is mixed inside the pipe and become more uniform. The uniformity is high on mid and tailpipe sensor location.

There is a different passive scalar distribution between SCR 1 and SCR 2. The SCR 1 has a NOx uniformity almost equal to 50% of the total section; it can be considered a good

approximation of NO_x distribution. Instead, SCR 2 has a lower distribution (<1%); without evaluate the chemistry of SCR this could or could not be a good approximation of NO_x distribution. The surface average of passive scalar for the two sections was computed and the resultant value is equal to 0.23. This mean that, if the NO_x leave the SCR with a binary distribution (1 → NO_x, 0 → no NO_x), the value of the passive scalar on sensor location should be equal to 0.23 (target value). Therefore, it is possible to evaluate the surface average on sensor section and compare the results obtained.

Tabella 9 Results passive scalar and uniformity on different section

| | Sensor 1 | Sensor 15 cm | Sensor 30 m | Sensor TP |
|--------------|----------|--------------|-------------|-----------|
| Surf Average | 0.253 | 0.251 | 0.24 | 0.23 |
| UI Scalar | 78.1% | 83.8% | 88.2% | 99.7% |

The values are quite near to the target; even if there are not much error, a qualitative interpretation can be done from this simulation. The mixing on sensor location is not enough and the measure here can be affected by error. An important role on this simulation is played by the almost total absence of NO_x from SCR 2. It would be interesting to evaluate a distribution comparable with the SCR 1 distribution (uniformity almost 50%).

Another possible simulation could be done making hypothesis on possible percentage of NO_x conversion and imposing the mass fraction of NO_x, but, as said, this is difficult without considering the chemistry of NO_x reduction.

Looking instead at the uniformity of passive scalar on sensor section, it is quite high for mid and tailpipe sensor, but it is near 78% for the section of the sensor. In the other sections the uniformity increase (84% on sensor located at 0.15 m from original NO_x sensor location and 87.5% on sensor at 0.3 m). These results confirm the simulation of tracer method for the evaluation of a coefficient of mixing, and confirm the experimental data.

Finally, another scene of the passive scalar target value can be plotted, using an isosurface derived part from STAR CCM+. The target value mainly starts from SCR 1 and develops inside the SCR canning, but it does not hit the sensor. The separation of fluid flow generated by the restricted area creates a velocity profile that transports the major quantity of NO_x in the centre of the pipe.

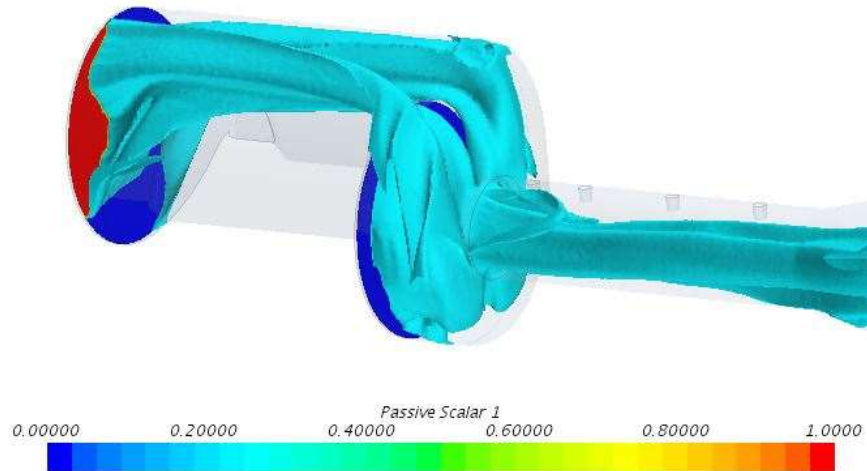


Figure 12.7 Isosurface passive scalar = 0.23

Looking the isosurface of the passive scalar, it is possible to see that, even if the NO_x develop inside the canning, the target value does not hit the sensor.

It would be interesting, as said, to evaluate another distribution of NO_x imposed at SCR 2 and then consider two passive scalars and evaluate distinctly the contribute of each one on sensor location (like it was seen using the tracer method for eight different passive scalars). In this way, it would be possible to evidence the grade of mixing for both SCR.

Maybe this is not the best method to analyse the real concentration of NO_x, but it can give a reasonable certainty for how and where the sensor would have less reading problems.

Conclusion

Create a predictive model that perfectly simulates the behaviour of NO_x on sensor location is not simple. The problem of NO_x sensor reading is quite important for the correct functioning of the system, for a great quantity of NO_x that is not detected can increase the pollution level in urban area. Also, high values of NO_x that are not able to mix inside the pipe are harmful to human health, and the ammonia slip generated from a malfunctioning of system is even worse than NO_x. The analysis and the studies done in this work attempted to find an appropriate methodology in order to solve the problem of NO_x sensor reading, following the two possible ways that can be investigated:

- Assess if the mixing of the fluid from SCR outlet to sensor location is strong enough to allow a correct lecture of NO_x;
- Assess if the distribution of NO_x on SCR outlet is good enough to simplify the mixing before reaching the sensor location.

The first way, was pursued using the passive scalar or tracer method, where arbitrary scalars, that does not interact with the fluid properties (passive), simulate the NO_x concentration coming from limited areas of the SCR outlet section. The purpose is to estimate, in the worst scenario, the grade of mixing of the scalars. The main problem of this method is the great dependency on boundary input condition. Surely enough, as seen, the choice of different shapes of the scalar influences considerably the results, whereas the number seems to have not much effects. The conclusion is that this method can be used as indicator of mixing inside the pipe, without confirming with absolute certainty if the sensor will or will not read correctly. Some target are defined by the company, but the author of this work has no information about how they were determined. To assess them, a lot of simulations and tests bench should be done in more conditions in order to completely study the method.

The second way, is a sort of real condition of the first analysis that influence the NO_x sensor reading. The real distribution of NO_x is strongly dependent on NH₃ uniformity at SCR inlet. This will vary from one system to another and with operating point. A more complete assessment of reality could be simulated with the injection of NH₃ and consequently evaluating the NH₃ uniformity at SCR inlet section. There are mainly two problems that concern this simulation:

- The first problem is that the real distribution of NH₃ on SCR inlet cannot be measured, there is no match with experimental data; the only thing that can be computed is the uniformity (must be high enough to assure a good NO_x conversion);
- The second problem is the sensitivity of distribution from model coefficients and input parameters, uniformity is case dependent. One more time, the problem is the same as the first point. Indeed, it is seen that high NH₃ uniformity gives good NO_x conversion, but real distribution of NH₃ is not simple to measure.

Simplified simulations and preventive hypothesis to avoid the chemistry were done, with the purpose of estimating a “real” distribution of NO_x. This real distribution was imposed at SCR outlet and simulated. The results shown, confirmed in another way the experimental data, but without a real value of NO_x concentration. A more complex model, with the introduction of chemistry, probably could provide results easily comparable with test bench measures. In addition, here, obviously, to develop such models a lot of experimental data would be necessary, but the final results would be a good predictive NO_x model.

Bibliography:

- [1] An Introduction to Computational Fluid Dynamics – The Finite Volume Method, Second Edition - H K Versteeg and W Malalasekera;
- [2] CD- Adapco Siemens. Star- CCM+ 13.06 User Guide.
- [3] Computational Methods for Fluid Dynamics, 3rd Ed, 2002 - Ferziger Peric;
- [4] Motori a combustione interna, Giancarlo Ferrari - 2016;
- [5] Numerical Computational of Internal and External Flows Volume 1 – Fundamentals of Computational Fluid Dynamics (Elsevier, 2nd ed, 2007) - Hirsch C.
- [6] Numerical Computational of Internal and External Flows Volume 2 - Hirsch C.
- [7] Turbulent Flows - Stephen B. Pope;
- [8] Ammonia Concentration Distribution Measurements on Selective Catalytic Reduction Catalysts, Rafal Sala, Jakub Dzida and Jaroslaw Krasowski, Article 1 June 2018 – Catalysts;
- [9] CFD Modeling of Tailpipe NOx Sensor Accuracy, Appor Kalyankar, Achuth Munnannur and Z. Gerald Liu, Article 10.4271/03-11-04-0029 - SAE International;
- [10] Formulation of the k-w turbulence model revisited. D.C. Wilcox. AIAA Journal, 46:359 – 375, 2011.